Life prediction model for creep-fatigue interaction of P92 advanced grade martensitic steel

A thesis submitted in the partial fulfillment for the award of the degree of

Master of Technology

in

Mechanical Engineering

(Specialization: Machine Design and Analysis)

Submitted by

RAJEEV KUMAR GUPTA

(Roll No: 212ME1514)

Department of Mechanical Engineering

National institute of Technology Rourkela - 769008, India

June-2014

National Institute of Technology

Rourkela

CSIR-National Metallurgical Laboratory

Jamshedpur

CERTIFICATE

*This is to certify that the thesis entitled, "**Life prediction model for creep-fatigue interaction of P92 advanced grade martensitic steel**" submitted by Mr. **Rajeev Kumar Gupta (212ME1514)** in partial fulfilment for the award of the degree of **Master Of Technology** in **Mechanical Engineering** with specialization in **Machine Design and Analysis** at National Institute of Technology, Rourkela (India) is authentic. Work carried out by him under my supervision and guidance.*

To the best of my knowledge, the matter embodied in the thesis has not been submitted to any other University / Institute for the award of any Degree or Diploma.

Dr. P. K. Ray

Professor

Department of Mechanical Engineering

National Institute of Technology

Rourkela-769008

Dr. J. K. Sahu

Principal Scientist

MST Division

CSIR-National Meatallurgical Laboratory

Jamshedpur-831007

ACKNOWLEDGEMENT

I would like to express my deepest and most sincere gratitude to my supervisors **Dr. J. K. Sahu**, Principal Scientist, MST Division, CSIR-NML, Jamshedpur and **Prof. P. K. Ray**, Professor, Department of Mechanical Engineering, N.I.T, Rourkela for his continuous guidance, encouragement and sharing valuable time throughout the process of this research work and in the preparation of this thesis. I also would like to express my sincere thanks to **Dr. S. Srikant** Director of CSIR-NML, Jamshedpur for providing valuable experimental facilities and **Prof**. **K.P.Maity** Head of the department, Mechanical Engineering for providing valuable departmental facilities.

I also thankful to research scholar Randhir Kumar Singh and Lalit Kumar Gupta staff of the CSIR-NML, Jamshedpur for his sincere co-operation during my research work.

Finally, I would like to thank my fellow post graduate students and the people who have been involved directly or indirectly in my endeavour.

Rajeev Kumar Gupta

Roll No: 212ME1514

Department of Mechanical Engineering

NIT Rourkela-769008

Abstract

Creep-fatigue interaction has been identified as a possible degradation mechanism leading to failure of power plant components such as thick sections header pipe etc. During startup/shutdown processes, severe thermal gradient sets in across the thickness between the inside and outside of the component. Fluctuation of demand also results in alternation of such operation results in thermal gradient. Both the above mentioned situation leads to hold time fatigue kind of situation. P92 (9Cr-1Mo-2W) martensitic steel is widely used for the manufacturing of header pipes and is subjected to creep-fatigue loading condition.

The aim behind the present study is to verify an existing unified viscoplasticity constitutive model, proposed by Choboche. This model includes combined isotropic hardening and kinematic hardening with a viscoplastic flow rule for time-dependent effects. For this study isothermal, uniaxial, fully reversed, strain controlled low cycle fatigue and stress relaxation fatigue tests at various hold time duration at maximum/minimum strain amplitude were conducted on P92 material at 600˚C. The P92 material in the present study has been recognized as a cyclic softening material

Here the initial value of material constants associated with Chaboche model has been determined from the first cycle stress-strain data, the maximum stress evolution during tests and the stress relaxation data. Then, the initial constants need to be optimized using a least-squares optimization algorithm in order to improve the general fit of the model to experimental data.

CONTENTS

CONTENTS

CHAPTER 1- INTRODUCTION

1.1. Background

The world today is moving in the direction of using ultra super critical technology (USC) to enhance the efficiency of fossil fired power plant up to 50%. The motivation behind this is the efficient utilization of indigenous coal available in abundance and at the same time to reduce the unwanted gas emissions. But the desired targeted efficiency of the power plant can be achieved by increasing the steam parameters (temperature and pressure) from 580°C and 290 bar to 630°C and 300 bar. But to sustain such higher steam conditions for a long time during service, the power plant component material should have adequate high temperature mechanical properties.

P92 (9Cr-Mo-2W) grade steel was introduced in the last decade as a candidate structural material for the steam generator components of fossil fired power plants [1]. The P92 grade has 25%-30% higher creep strength in comparison with P91 and possesses adequate mechanical properties, oxidation and corrosion resistance at high temperature and pressure.

The steam boiler components, during service, are often subjected to repeated thermal stresses as a result of temperature gradients that occur on heating and cooling during start-ups/shut-downs or during running condition [2]. Under steady state conditions time dependent creep or stress relaxation on the material are most likely to occur at high temperature. Therefore failure mechanisms under such loading conditions are a result of complex interactions of time-dependent creep damage and fatigue processes at elevated temperature.

Earlier research on these materials has focussed on its creep strength. However, as the current operation involves cyclic operation, the understanding of creep-fatigue interaction behaviour of these power plant materials has become more important for the prediction of component service life which is very important to avoid any catastrophic accident during service at elevated temperature. This life prediction can be done by finite element simulation. The simulation of the components requires a suitable constitutive material model which can accurately predict the stress-strain behaviour and the failure life during cyclic loading conditions. The majority of previous studies on power plant materials have been related to the creep behaviour under constant load operation. For example, creep constitutive equations have been developed for the parent, heat-affected zone (HAZ) and weld materials of Cr-Mo-V steel welds

in the range 565-640˚C [3]. The development of these creep constitutive models has contributed to the gaining of a better understanding of the material behaviour in such applications [4].

In contrast to the above applications, the constitutive models which deal with creep and cyclic loading conditions of power plant materials have had relatively little attention. Thus, a model which can include both cyclic and viscous effects is required. A commonly used model is the unified viscoplasticity model originally developed by Chaboche [5]. This viscoplasticity model has been used by many researches on aero engine materials such as nickel-base alloys [4]. However, this model is rarely used to represent the behaviour of power plant materials.

1.2. Objectives

The objectives of the research are:

- To understand the viscoplastic constitutive model.
- To obtain stress-strain data for P92 steel by conducting low cycle fatigue and creep-fatigue interaction test for various hold durations at 600^{o}C in air.
- To investigate the cyclic softening behaviour of the steels by analyzing the stress-strain behaviour throughout the lifetime of the steel.
- To find out P92 material constants to form a constitutive model that may predict creep and cyclic plasticity behaviour in high temperature environment.

1.3. Work plan:-

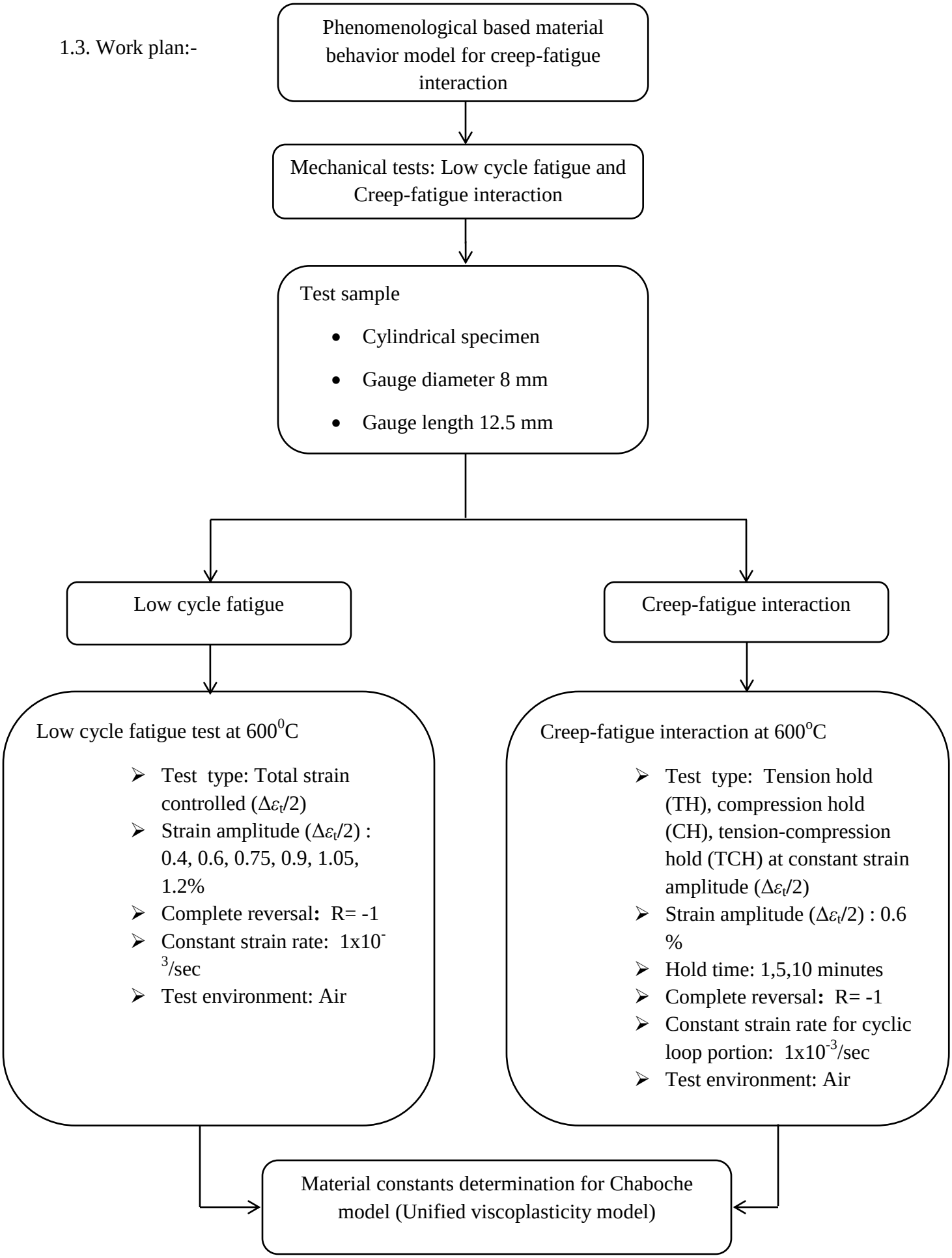
Phenomenological based material behavior model for creep-fatigue interaction
Mechanical tests: Low cycle fatigue and Creep-fatigue interaction
Test sample
Cylindrical specimen
Gauge diameter 8 mm
Gauge length 12.5 mm
Low cycle fatigue
Creep-fatigue interaction
Low cycle fatigue test at 600^{0}C
Test type: Total strain controlled ($\Delta\varepsilon_t/2$)
Strain amplitude ($\Delta\varepsilon_t/2$) : 0.4, 0.6, 0.75, 0.9, 1.05, 1.2%
Complete reversal: R= -1
Constant strain rate: 1x10^{-3}/sec
Test environment: Air
Creep-fatigue interaction at 600^{o}C
Test type: Tension hold (TH), compression hold (CH), tension-compression hold (TCH) at constant strain amplitude ($\Delta\varepsilon_t/2$)
Strain amplitude ($\Delta\varepsilon_t/2$) : 0.6 %
Hold time: 1,5,10 minutes
Complete reversal: R= -1
Constant strain rate for cyclic loop portion: 1x10^{-3}/sec
Test environment: Air
Material constants determination for Chaboche model (Unified viscoplasticity model)

CHAPTER 2- LITERATURE REVIEW

2.1 Overview

This chapter is mainly concerned with material constitutive models for the steels used in this study, namely P92 steels. The steels which is specifically used in the power plant applications deforms cyclically under thermo-mechanical fatigue loading conditions, so plastic behaviour associated with strain hardening behaviour of the material becomes important. The strain hardening behaviour during time independent cyclic loading is defined in terms of isotropic and kinematic hardening. So this chapter includes review of these hardening rules. This chapter also includes details of the development of the P92 steels.

2.2. Introduction to material behaviour modeling

Basically a material behaviour model is used to describe the stress-strain behaviour of a material. There are two classes of material behaviour modeling:

a) Physically-based model: In this model the mechanical behaviour is represented by considering microstructure evolutions of materials. This kind of model is used to represent both microscopic phenomena, such as microstructure evolution, and macroscopic mechanical behaviour, such as creep and relaxation, on a material. For example, cyclic softening behaviour of the martensitic 9Cr1Mo steel has been modelled by analyzing and measuring the dislocation density using transmission electron microscopy; the microstructure size and the macroscopic stresses of cyclic softening phenomenon can then be predicted [6-7].

b) Phenomenological-based model: This model is based on the results of mechanical tests on a material. This material model is used to predict the stress-strain behaviour of a material and the model can be further used to predict the stress-strain behaviour of a mechanical structure using a finite element simulation. The second model will be the focus of the study here.

2.3 Elastic and plastic deformation

When a load is applied on a component, the material will deform either in elastic manner or in elastic-plastic manner, which depends on the magnitude of the applied load. The material which deform within the elastic range will return to its original shape when the load is removed. On the

other hand, plastic deformation is irreversible and occurs when the load applied on the component exceeds its elastic limit. In terms of the physics of the phenomena, the elastic deformation involves a variation in the interatomic distances without changes of place while plastic deformation modifies interatomic bonds caused by slip movement in the microstructure of the material [8].

When a load is applied on a component within its elastic limit, the magnitude of the extension was found to be proportional to the applied load. Thus, the deformation of an elastic deformation is described mathematically in terms of stress (σ) which refers to the ratio of the applied force to the cross sectional area, and strain (ε) which refers to the ratio of the extension to the initial length by the following equation:

$$F = kx \qquad 2.1$$

Where, F is applied force, x is associated displacement and k is the proportionality factor.

Based on equation 2.1, the force and the displacement characteristics depend on the size of the measured body. Thus, stress, σ, which refers to the ratio of the applied force to the cross sectional area, and strain, ε, which refers to the ratio of the extension to the initial length, are introduced to eliminate the geometrical factors. So the equation 2.1 can be rewritten as:

$$\sigma = E\varepsilon \qquad 2.2$$

Where, E is proportionality constant which is often referred to as the Young's modulus or the modulus of elasticity for the material. Equation 2.2 is also known as Hooke's law, which describes the linear stress-strain response of a material.

Plastic deformation occurs when the applied load (or stress) exceeds a certain level of stress called the elastic limit. Above this limit, the stress is no longer proportional to strain. However, the exact stress at which this limit occurs is difficult to determine experimentally as it depends on the accuracy of the strain measurement device used. Thus, a conventional elastic limit or a yield stress value is determined by constructing a straight line parallel to the linear elastic stress-strain curve at a specified strain offset of 0.2%. The intersection point between the parallel line and the experimental curve is taken as the yield stress (0.2% proof stress) value. For example, the yield

stress value of P92 steel at 600°C temperature with a 0.2% offset criterion is 302.58 MPa as shown in figure 2.1

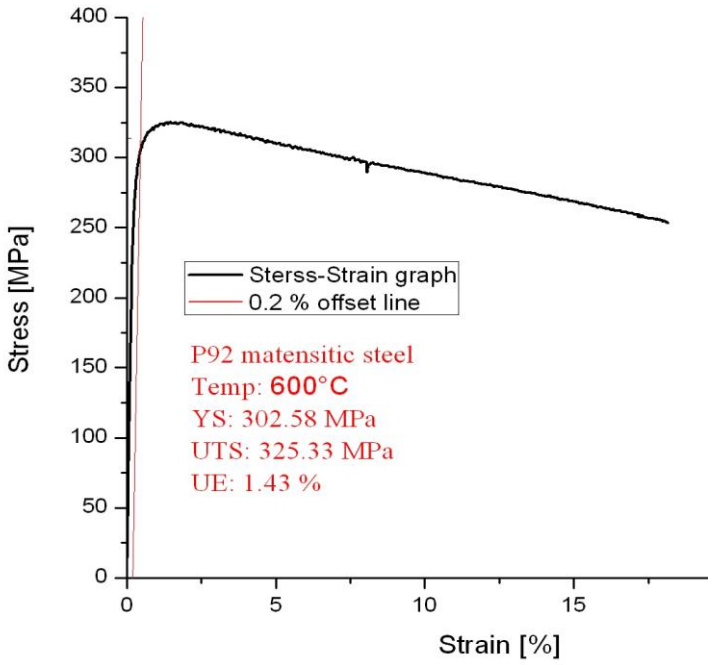

Figure 2.1: Tensile test graph for P92 steel at 600˚C

Inelastic deformation under creep: Irreversible deformation may also occur at stresses below the elastic limit if the load is maintained for a long time. This type of deformation is referred to as creep, the magnitude of which is a function of stress, time and temperature. The creep effect is significant at high temperatures and is generally significant when the temperature of the material is greater than approximately 0.4 of the absolute melting temperature (T_m). A creep test is conducted by applying a constant load to a specimen, which results in three stages of creep deformation. In the primary stage, the strain rate decreases with time as the material approaches a steady-state stage. The creep strain increases steadily in the secondary stage with a constant (minimum) strain rate. Finally, the strain rate accelerates during tertiary creep until final failure occurs [9-10]. The secondary stage of creep usually occupies the longest period of time in a creep test and the steady-state creep rate behaviour is usually expressed by a power law, also referred to as Norton's law, which is given by the following equation

$$\dot{\varepsilon} = A\sigma^n \qquad 2.3$$

Where, A and n are material constants which can be determined from data obtained in the secondary stage.

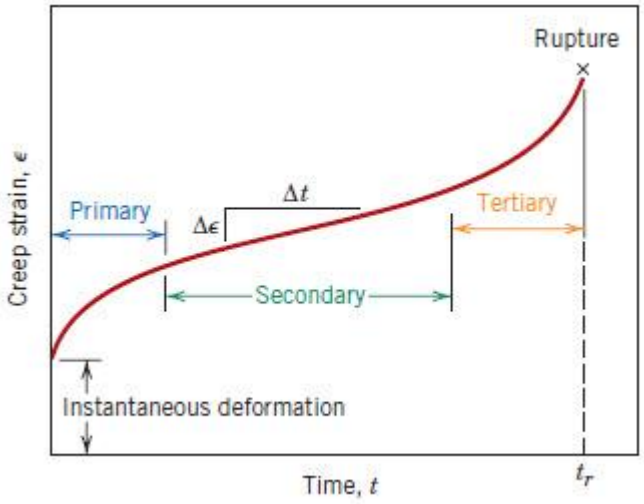

Figure 2.2: A schematic diagram of creep curve

2.4 Cyclic plasticity

When a component is subjected to cyclic loading, the plastic deformations which occur in the material exhibit several phenomena such as the Bauschinger effect, cyclic hardening/softening and material ratchetting. The cyclic loading of a material, under tension-compression conditions, produces a hysteresis loop. The stress-strain behaviour which occurs under cyclic loading, with time independent effects are normally represented by isotropic hardening, kinematic hardening or some combination of both the isotropic and kinematic hardening models.

2.4.1. Isotropic hardening model

Isotropic hardening describes the change in the size of the yield surface, as a function of accumulated plastic strain. A schematic description of the isotropic hardening model is shown in Figure 2.3.

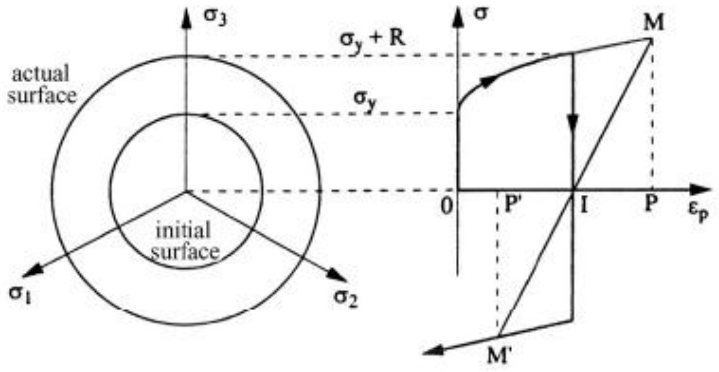

Figure 2.3: Schematic representation of isotropic hardening on the deviatoric plane and in tension-compression test conditions [11]

Isotropic hardening, or alternatively, the change in the size of the yield surface is represented by a scalar variable, R, which is also known as drag stress [5]. The rate of evolution of isotropic hardening is represented by the following equation:-

$$\dot{R} = b(Q - R)\dot{p} \qquad 2.4$$

Where p is the accumulated plastic strain, Q is the asymptotic value of R and b define the speed at which the saturation value, when variable R is constant, is approached. Equation 2.4 can be integrated with respect to time to give the following equation:-

$$R = Q(1 - e^{-bp}) \qquad 2.5$$

By using the von Mises loading function, the yield criterion for the isotropic hardening model, in the uniaxial form, is given in the following equation:-

$$f = |\sigma| - R - \sigma_Y = 0 \qquad 2.6$$

Where, σ_Y is the initial uniaxial yield stress in tension or the initial elastic limit, as shown in Figure 2.3.

Cyclic hardening/softening: Under cyclic loading conditions, an undamaged material (in which cracks do not generally influence the mechanical behaviour) exhibits an evolution of the plastic

strain range as the number of cycles increases which is referred to as cyclic hardening or cyclic softening behaviour. The cyclic hardening of a material refers to the decrease of the plastic strain range, associated with an increase of the stress amplitude with increasing number of cycles in a cyclic test. This is observed under strain-controlled test conditions. This behaviour has been observed in many materials such as 316 stainless steel [12-14], high nickel-chromium materials [15] and nickel-based superalloys [16-18]. On the other hand, the plastic strain range increases as cyclic loading continues in a material, exhibiting cyclic softening behaviour such as is found to occur in a 55NiCrMoV8 [19] and 9Cr-1Mo steel [20-23]. The cyclic hardening phenomenon indicates an increase of material's strength [11] in which the elastic strain range increases for a constant strain range. In the isotropic hardening model, this phenomenon is represented by an increase of the elastic limit ($R + \sigma_Y$). For a material exhibiting cyclic softening behaviour, the constant Q is negative so that a stabilized yield surface becomes smaller than the initial one [11].

2.4.2. Kinematic hardening model

The hardening of a material, which occurs due to plastic deformation, can also be represented by use of a kinematic hardening model. In this model the yield surface translates in stress space, rather than expand [24]. The kinematic hardening parameter χ is a tensor, also called the backstress [5], which defines the instantaneous position of the loading surface [8]. Figure 2.3 is a schematic description of the kinematic hardening model in stress space and the corresponding model in a tension-compression test, in which k represents elastic limit value.

Bauschinger effect: In a tension-compression test, it is typically found that the yield stress in compression is lower than that if the test was carried out in tension first. This behaviour is known as the Bauschinger effect in which plastic deformation increases the yield strength in the direction of plastic flow and decreases it in the reverse direction [25]. The kinematic hardening model is more appropriate for representing this phenomenon where the model assumes that the elastic region remains constant, both initially and during cyclic loading [24], as illustrated, schematically, in Figure 2.4. The kinematic hardening model can be used in predicting the Bauschinger effect [26].

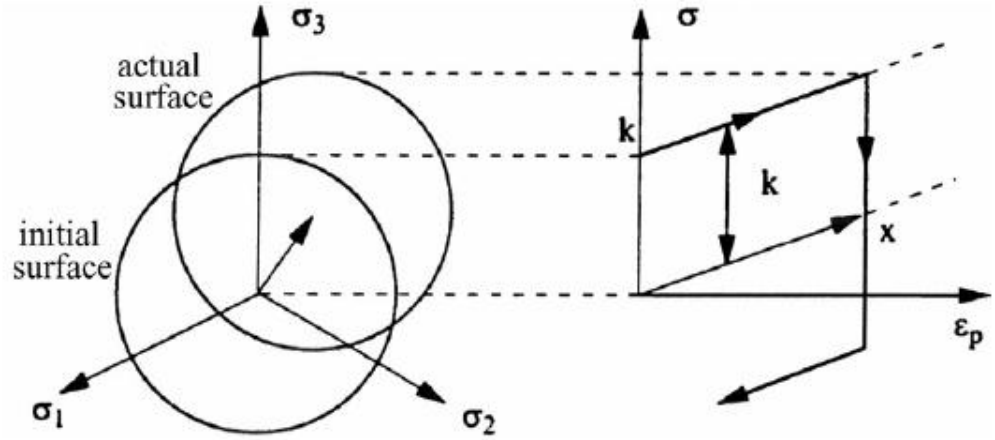

Figure 2.3: Schematic representation of kinematic hardening in deviatoric plane and in tension-compression test [11]

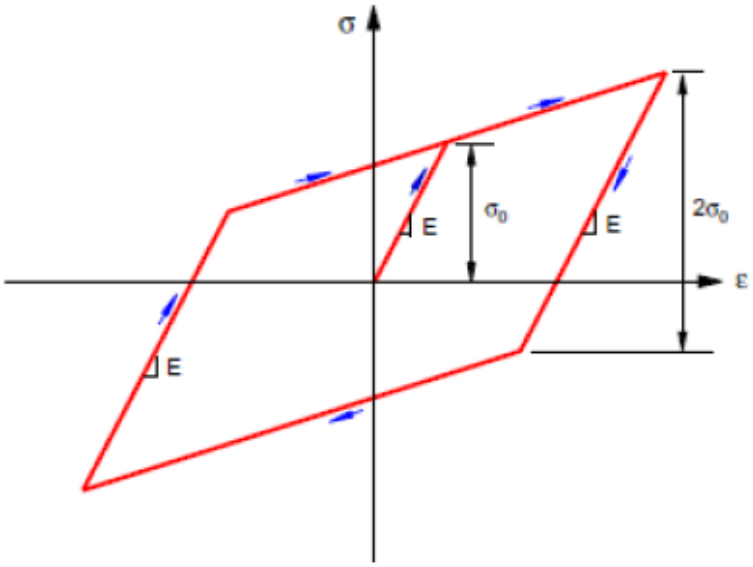

Figure 2.4: Schematic illustration of the Bauschinger effect in which the elastic limit is represented by $\sigma_0$in this figure [25]

The yield criterion for the kinematic hardening model, in the uniaxial form, is given by the following equation:-

$$f = |\sigma - \chi| - k \qquad 2.7$$

Where, k is the initial yield stress value. In the kinematic hardening model, the initial yield stress is also described as the initial elastic limit or the initial size of the yield surface [8, 27].

The simplest model used to describe kinematic hardening uses a linear relationship between the change in kinematic hardening and the change in plastic strain. The linear kinematic hardening model, originally developed by Prager [28], is given by the following equation:-

$$\dot{\boldsymbol{\chi}} = \frac{2}{3} c \dot{\boldsymbol{\varepsilon}}_p \qquad 2.8$$

Where, c is the material constant, which represents the gradient of the linear relationship [29]. For the uniaxial loading case, Equation 2.8 is given by the following:-

$$\dot{\chi} = c \dot{\varepsilon}_p \qquad 2.9$$

Where, χ represents a scalar variable; the magnitude of χ is 3/2 times the kinematic hardening tensor parameter [24]. But in the actual cyclic loading test linear strain hardening is rarely observed. Generally, the stress-strain behaviour obtained from cyclic loading tests is a nonlinear relationship. The Amstrong-Frederick type kinematic hardening model, originally developed in 1966, has been used widely to represent this nonlinear stress-strain relationship. The model introduces a recall term, called dynamic recovery, into the linear model [30] which is given by the following equation:-

$$\dot{\boldsymbol{\chi}} = \frac{2}{3} c \dot{\boldsymbol{\varepsilon}}_p - \gamma \boldsymbol{\chi} \dot{p} \qquad 2.10$$

Where, γ is a material constant. The recall term incorporates a fading memory effect of the strain path and causes a nonlinear response for the stress-strain behaviour [31]. For the nonlinear kinematic hardening model of the time-independent plasticity behaviour, the value of γ / c determines the saturation of stress value in the plastic region and its combination with the k value represents the maximum stress for the plasticity test [24]. The saturated stress is described, schematically, in Figure 2.5.

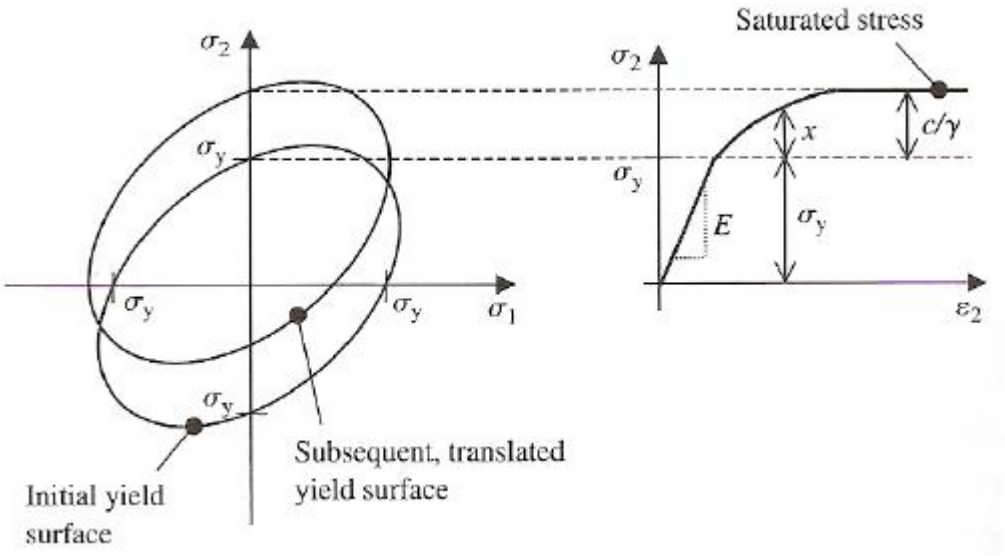

Figure 2.5: Schematic representation of saturated stress represented by the nonlinear kinematic hardening model (Dunne and Petrinic, 2005)

The constants in the nonlinear kinematic hardening model are represented by different equation than that in equation 2.10 [5]. The equation is given as follows:-

$$\dot{\chi} = C\left(\frac{2}{3}a\dot{\varepsilon}_p - \chi\dot{p}\right) \qquad \textbf{2.11}$$

Where *a* is the saturation of the stress value in the plastic region, which is identical to the value of *c/* γ, and *C* represents the speed to reach the saturation value, which is equal to γ. In general, both of the nonlinear kinematic hardening equations (2.10 and 2.11) are the same, except for the fact that the constants are different in definition.

The Amstrong-Frederick hardening relation has been modified by decomposing the total backstress into a number of additive parts [32]. The reason for the superposition of the kinematic hardening model is to extend the validity of the kinematic hardening model to a larger domain in stress and strain [5]. The model is also intended to describe the ratchetting behaviour better [8]. Thus, the total backstress χ is given by the following equation:

$$\chi = \sum_{i=1}^{M} \chi_i \qquad \textbf{2.12}$$

Where, χ_i is a part of the total backstress, i = 1,2,…,M and M is the number of the additive components of the kinematic hardening. The model is usually decomposed into two or three

kinematic variables. However, more variables are sometimes employed in certain cases, for example, in the study of the ratchetting effect [31], in order to get a better agreement with experimental data. It is suggested by Chaboche [33] that the first rule (χ_1) should start hardening with a very large modulus and that it stabilizes quickly. For example, the superposition of three kinematic hardening variables is shown in Figure 2.6.

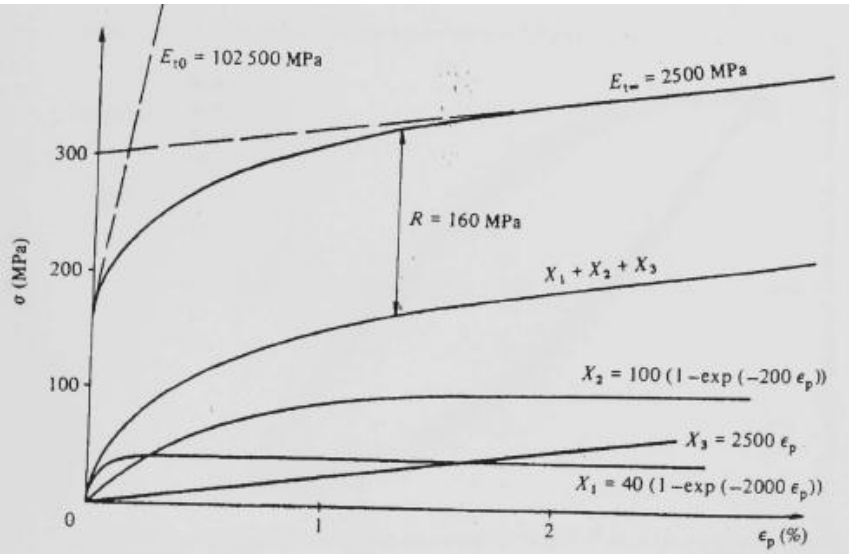

Figure 2.6: The stress-strain curve obtained from the superposition of three kinematic hardening variables [8]

2.4.3 Combined isotropic-kinematic hardening model

Both the cyclic hardening/softening and Bauschinger phenomena are normally observed in tests of the real material. This observation indicates the requirement to combine both isotropic and kinematic hardening rules in order to predict the strain hardening and the cyclic hardening/softening of engineering materials. The yield criterion of the combined isotropic and kinematic hardening models, in the uniaxial form, is given by the following equation:-

$$f = |\sigma - \chi| - k - R \qquad 2.13$$

Theoretically, the behaviour of the material with a combined isotropic and kinematic hardening model will include both the translation and the expansion/contraction of the yield surface in stress space [34]. In this paper, the author used a time independent cyclic plasticity model combined with isotropic hardening and two nonlinear kinematic hardening rules, to predict the behaviour of a nickel base superalloy, at 300°C.

2.5 Time-dependent cyclic plasticity

The repeated loading of engineering components at high temperature may involve both plasticity and creep behaviour. The constitutive model for this condition is known as a time-dependent or a rate-dependent plasticity in which the plastic strain and the creep strain contribute to the total strain value.

2.5.1 Uncoupled elastoplasticity-creep

Conventionally, the creep (time-dependent) and the plasticity (time-independent) behaviour are modelled by an uncoupled elastic-plasticity-creep model. In the model, the stress-strain behaviour is represented by a creep model such as the Norton's law and by a typical plasticity model such as the isotropic and kinematic hardening models. For example, Shang et al. [35] used the model to represent the behaviour of superplastic forming dies. The constants for the selected creep and plasticity models are determined separately in a constant loading test and in cyclic loading tests, respectively, and there is no interaction assumed to occur between those constants in the creep and plasticity equations. In certain conditions, particularly for cyclic creep (ratchetting effect) and creep-plasticity interaction, the combination of the plasticity and creep equations give unsatisfactory results when compared to experimental data [36]. Thus, a viscoplasticity model has been used more frequently than the uncoupled elastic-plasticity-creep model to describe time-dependent plasticity behaviour at high temperature.

2.5.2 Unified viscoplasticity model

A viscoplasticity model refers to the mechanical response of materials in plastic condition which exhibits time dependent effect represented by a viscosity function [37]. A well known viscoplasticity model is the unified viscoplasticity model proposed by Chaboche [5]. The model is known as the "unified" viscoplasticity model for two reasons [27]. Firstly, the plastic and the creep strains are represented simultaneously by one parameter and these strains are called the viscoplastic strain. Consequently, the strain does not exhibit a discontinuity under different types of loading. Secondly, the same hardening rules as the time independent plasticity rule are employed in the viscoplasticity model.

The viscoplastic strain rate of the model, in the uniaxial form is given by the following equations:-

$$\dot{\varepsilon}_p = \left\langle \frac{f}{Z} \right\rangle^n \operatorname{sgn}(\sigma - \chi) \qquad 2.14$$

$$\operatorname{sgn}(x) = \begin{cases} 1, x > 0 \\ 0, x = 0 \\ -1, x < 0 \end{cases} \quad \text{and} \quad \langle x \rangle = \begin{cases} x, x \geq 0 \\ 0, x < 0 \end{cases} \qquad 2.15$$

$$f = \left| \sigma - \chi \right| - k - R \qquad 2.16$$

In the unified viscoplasticity model, the total stress can be decomposed into four parts, namely initial yield stress (k), drag stress (R), backstress (χ) and viscous stress (σ_v) as given by the following equation:-

$$\sigma = \chi + (R + k + \sigma_v) \operatorname{sgn}(\sigma - \chi) \qquad 2.17$$

The viscous stress which represents the rate dependency of the stress is a power function of the accumulated plastic strain rate as follows:-

$$\sigma_v = Z\dot{p}^{1/n} \qquad 2.18$$

The viscous stress is also known as the overstress due to the fact that the viscoplastic formulation allows the stress state to overpass the purely elastic domain [38]. A schematic representation of the total stress decomposition in the unified viscoplasticity model is shown in Figure 2.7.

The unified viscoplasticity model has been used by Tong and his co-workers to predict the stress-strain behaviour of a nickel-based superalloy. For example, Zhao et al. [34] developed the unified model to predict the stabilized cyclic loops of a nickel base superalloy at various strain ranges and at high temperatures. At the beginning of the work, only one strain rate was used in the study. An optimisation method was used to improve the initially determined parameters by minimizing the difference between the predicted and the experimental stress values. The optimisation method was further improved by considering several types of test data in the optimisation process such as monotonic, cyclic, relaxation and creep test data [39-40] and this process resulted in better predictions for the cyclic and creep tests by using only a single inelastic strain variable within the model. Additional terms can be included in the model such as a static recovery term [16] and a plastic strain memory term [41] in order to improve the model's prediction for more complex stress-strain behaviour. It can be seen from the works of Tong and his co-workers that the viscoplasticity model for the nickel-based superalloy has been developed

in several stages, starting from a simple model, and the optimization program has been used to determine the material constants.

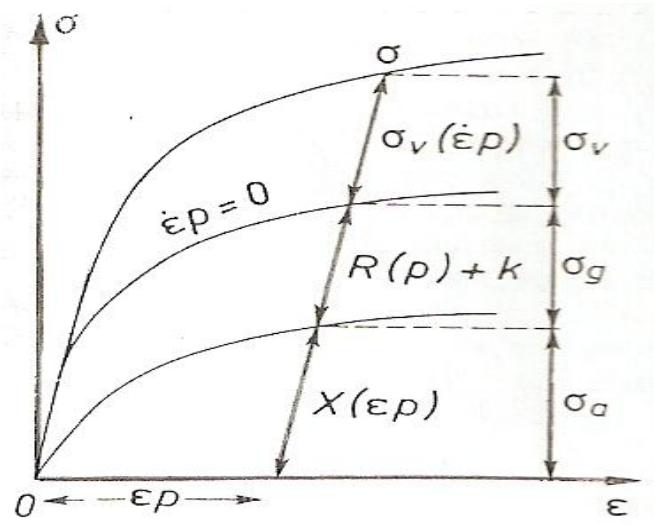

Figure 2.7: The decompositions of stress in the tensile test according the unified viscoplasticity model [5]

2.6 P92 grade steel

2.6.1 Introduction to P92 grade steel

In the power generating industry, the economic efficiency of power plant operation has been improved by designing better power plant structures and by developing new steels with better properties. The creep properties of power plant materials have been of major concern to material scientists due to the need to operate the power plants at high temperatures over long periods of time. The steels used in conditions are known as creep-resistant steels. Examples of creep resistant steels are P91 and P92 steels. In power plant application, the steels have been used in superheater and reheater tubes and also in the headers and in the steam piping at high temperatures, as shown in Figure 2.8. In general, P91 steel consists of 9% chromium and 1% molybdenum while P92 steel consists of 9% chromium, 1.75% tungsten and 0.5% molybdenum [42]. The steels are ferritic/martensitic type steels which are commonly grouped as 9-12%Cr steels. The ferritic type of steel has a lower thermal expansion coefficient value, as compared to an austenitic type steel [43], which is an advantage for the ferritic type steel when dealing with thermal fatigue problems.

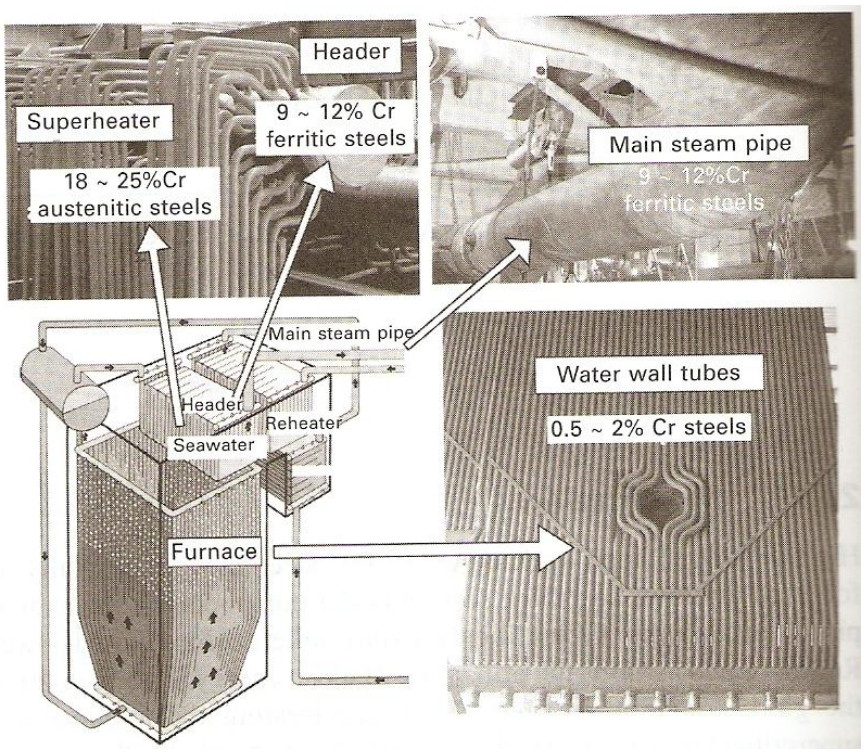

Figure 2.8: Schematic illustration and photographs of a fossil fired boiler and typical materials [48]

The demand for ferritic steels with higher creep strength has contributed to the development of 9Cr martensitic steel [2]. P91 steel was originally developed by Oak Ridge National Laboratory (ORNL) in the late 1970s as a modification to 9Cr-1Mo steel [44]. The modification consisted of the addition of vanadium, niobium and nitrogen and also the reduction of carbon, chromium, silicon, molybdenum, phosphorus and sulphur content [45]. Thus, the steel is also known as modified 9Cr-1Mo steel. P91 steel has been used in the UK power industry, either in retrofit or new build applications [46]. P92 steel was originally developed under Nippon Steel's program in 1990s [43]. The steel was developed in order to improve the P91 steel behaviour by adding tungsten (W) and boron (B) content and reducing the molybdenum content [42]. The P92 steel has better creep strength by approximately 10-20% compared with P91 steel; thus, P92 pipe wall thicknesses can be reduced, resulting in improved behaviour of the steel under thermal fatigue situations [47]. The chemical compositions in accordance with ASTM standard, for P91 and P92 steels are given in Table 2.1.

Table 2.1: Chemical composition of P91 and P92 steels (in wt. %) [47]

Steel Grade	C	Cr	Mo	W	Mn	Nb	V	Ni	Si	Al	S	P
P91	0.11	9.23	0.98	----	0.38	0.09	0.25	0.13	0.35	0.02	0.007	0.029
P92	0.09	9.34	0.58	1.76	0.48	0.06	0.21	0.14	0.15	0.005	0.012	0.20

In general, 9-12%Cr steels are heat treated, which consists of an austenitizing and tempering procedure, during their manufacturing, in order to meet the requirements of the steel's specifications. The steel is austenised at a temperature around 1100°C. The cooling process, from austenizing temperature to room temperature, produces a martensitic structure with a high dislocation density. Then, the steel is tempered at temperature at around 750°C in order to improve the ductility and impact strength. Subgrains and dislocation networks are formed during tempering [43]. Different temperatures and periods of heat treatments are reported in the literature for 9-12%Cr steels [23]. The different parameters used for the austenitizing and tempering processes can affect the microstructure of the steels. For example, selecting a high austenitising temperature results an increase in the lath width and an increase in the prior austenite grain size [43]. The variation in heat treatment can also result in slight differences in mechanical properties.

CHAPTER 3 - EXPERIMENTAL WORK

3.1 Experimental

3.1.1 Material

The steel used in the present study are P92 grade steel (9Cr-Mo-2W) used in superheater and reheater tubes and also in the headers and in the steam piping at high temperatures. The chemical composition of the P92 steel employed in this study is given in Table 3. Cylindrical specimens with a gauge diameter of 8 mm and a gauge length of 12.5 mm were used for high temperature low cycle fatigue and creep-fatigue interaction investigation.

Table 3.1

Chemical Composition of P92 Steel (in wt. %)

C	Cr	Mo	W	Mn	Nb	V	Ni	Si	Al	S	P
0.09	9.34	0.58	1.76	0.48	0.06	0.21	0.14	0.15	0.005	0.012	0.20

3.2 Testing procedures for the P92 steel

The aims of the tests are to obtain the stress-strain behaviour of the material so that a constitutive material behaviour model can be developed based on these data. The test loading conditions were based on the high temperature requirement of power plant and to produce a deformation which will give plastic behaviour. Here isothermal tests of P92 specimens were conducted at 600°C. The strain amplitude value was selected to ensure that significant plasticity would occur with this amplitude. Several strain-controlled low cycle fatigue tests, with the same strain rate, were performed at 600°C with various strain amplitudes. Using the same strain amplitude at particular temperature, tests with a hold period, in tension/compression/both, for 1, 5 and 10 minutes were performed in order to study the time-dependency effect. The duration of hold period was chosen so that constant rate of stress drop, in each cycle, was recorded in the test.

Actions performed prior to starting the test

Prior to starting up each test, load and strain calibration of the testing machine system was performed in order to obtain a load and strain variations within the gauge length.

In order to obtain a good response for a specified test loading, the PID (proportional, integral, derivative) values of the testing machine system were tuned. The strain

amplitudes and testing periods for the actual tests were applied on a specimen and the PID values were adjusted accordingly to get a good fit to controlled shape parameter (strain, load or position). The PID values for the P92 steel tests are determined by trial-and-error process.

The temperature of the specimen during the test was measured by using thermocouples (TC). Two R-type thermocouples were used in each test. The thermocouple wires were attached manually at top and bottom of the specimen surface and the distance between the two thermocouple wires must be more than specimen gauge length.

3.2.1 LCF experiment

Low cycle fatigue (LCF) tests were performed as per ASTM E 606 standard under fully reversed total axial strain control mode employing a triangular waveform. Tests were conducted at 600˚C at a constant strain rate of $1x10^{-3}$ s^{-1} with various total strain amplitudes ($\Delta\varepsilon_t/2$) 0.25%, 0.4%, 0.6%, 0.75%, 1.05% and 1.2%. Two external thermocouples were tied on the specimen for continuous temperature measurement during the progress of the test. The gauge length of the high temperature extensometer used in the fatigue tests is 12.5 mm and has a travel of ±20%. The tests were interrupted at the onset of visible cusping in the hysteresis loop for all applied values of $\Delta\varepsilon_t/2$ and the number of cycles till then is considered to be the cyclic life (N_f) of the material. The cusping provides us the indication of the crack initiation at the specimen surface within the gauge length and the test is needed to stop now. Sudden load drop for the second time in the load vs cycle graph also indicates the crack initiation at the specimen surface. For the fatigue tests where cyclic saturation was not observed, hysteresis loop corresponding to mid-life ($N_f/2$) is considered for calculation of plastic strain amplitude and stress amplitude at saturation. These values are used for constructing the Coffin-Manson plot and the cyclic stress strain curve. Figure 3.1 shows the typical curves obtained during a strain-controlled LCF test.

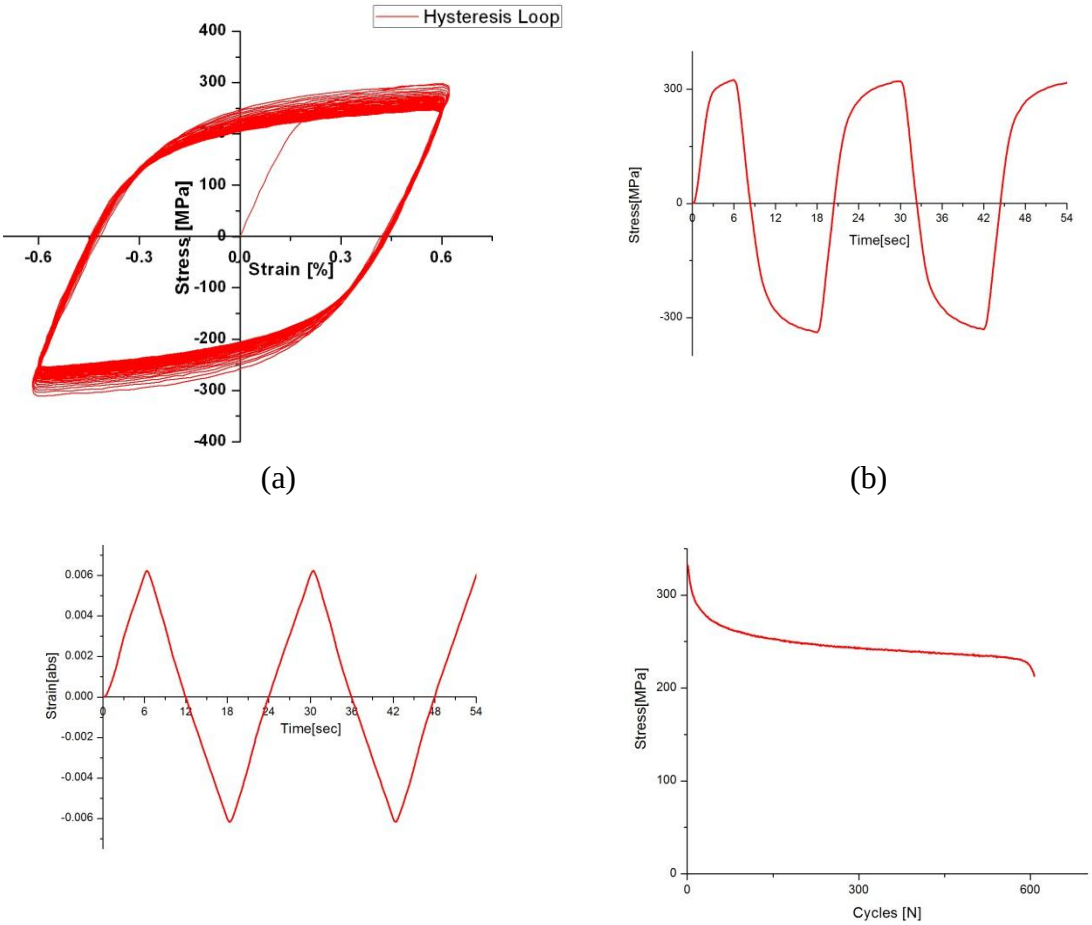

Figure 3.1: Types of graphs obtained during strain controlled low cycle fatigue test: ($\Delta\varepsilon_t/2$ = 0.6%, strain rate: 10^{-3}/sec, R = -1, Temperature: 600°C, Test environment: Air.

a) Stress (σ) vs Strain (ε) (Hysteresis loop); b) Stress (σ) vs Time; c) Strain (ε) vs Time; d) Stress amplitude vs number of cycles

Important parameters such as stress range ($\Delta\sigma$); plastic (or inelastic) strain range ($\Delta\varepsilon_p$); total strain range ($\Delta\varepsilon_t$) (which is the controlled parameter in the test) and elastic strain range ($\Delta\varepsilon_e$) can be identified from the stress-strain hysteresis loop as shown in Figure 3.2.

P92 steels, as shown in the Figure 3.3, exhibit cyclic softening behaviour in which stress amplitude decreases as the number of cycle increases. Generally, the behaviour in fatigue loading tests is associated with the increase of plastic strain range in a material as a result of continuous cyclic loading. Figure 3.4 shows the evolution of plastic strain range observed in the tension-compression test of P92 material. It can be seen from the graph that the plastic strain

range increase rapidly during the initial stage and then become stable after approximately a quarter of the total number of cycles.

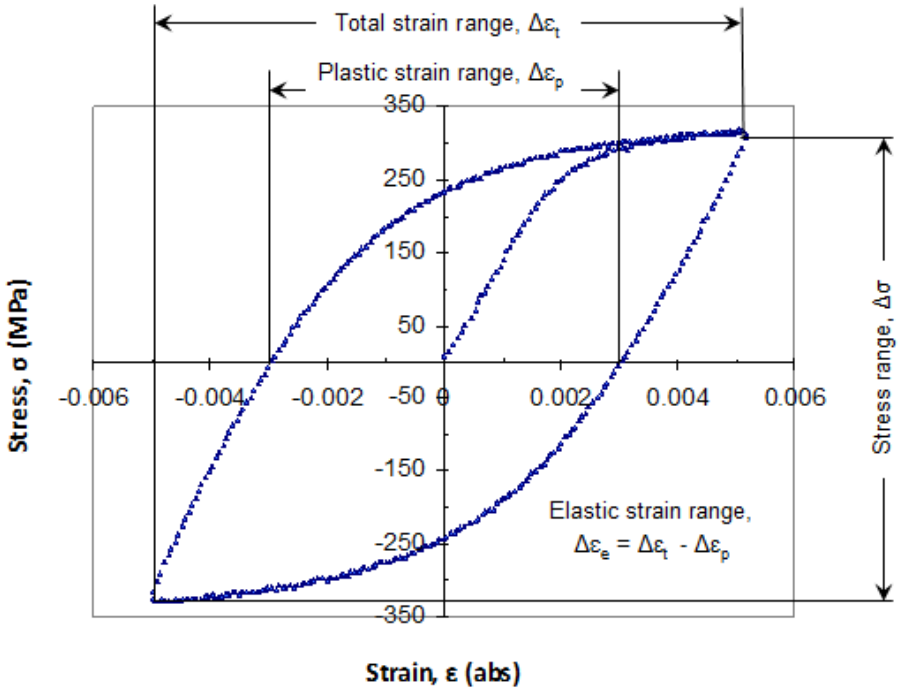

Figure 3.2: Example of typical stress-strain hysteresis loop and the parameters determined from the loop for an isothermal strain-controlled test

Table 3.2

Fatigue test parameters of LCF tests, cyclic life, stress amplitude and plastic strain amplitude values at $N_f/2$ cycles. All tests were conducted at strain rate $1x10^{-3}$/s.

LCF test temperature	$\Delta\varepsilon_t/2$	N_f	$\Delta\sigma/2$ at $N_f/2$ cycles [MPa]	$\Delta\varepsilon_p/2$ at $N_f/2$ cycles
600˚C	2.5×10^{-3}	8046	207	1.00×10^{-3}
600˚C	4×10^{-3}	2321	230	2.32×10^{-3}
600˚C	6×10^{-3}	582	256	4.54×10^{-3}
600˚C	7.5×10^{-3}	481	245	5.51×10^{-3}
600˚C	9×10^{-3}	285	265	7.27×10^{-3}
600˚C	10.5×10^{-3}	349	261	8.41×10^{-3}
600˚C	12×10^{-3}	196	259	10.09×10^{-3}

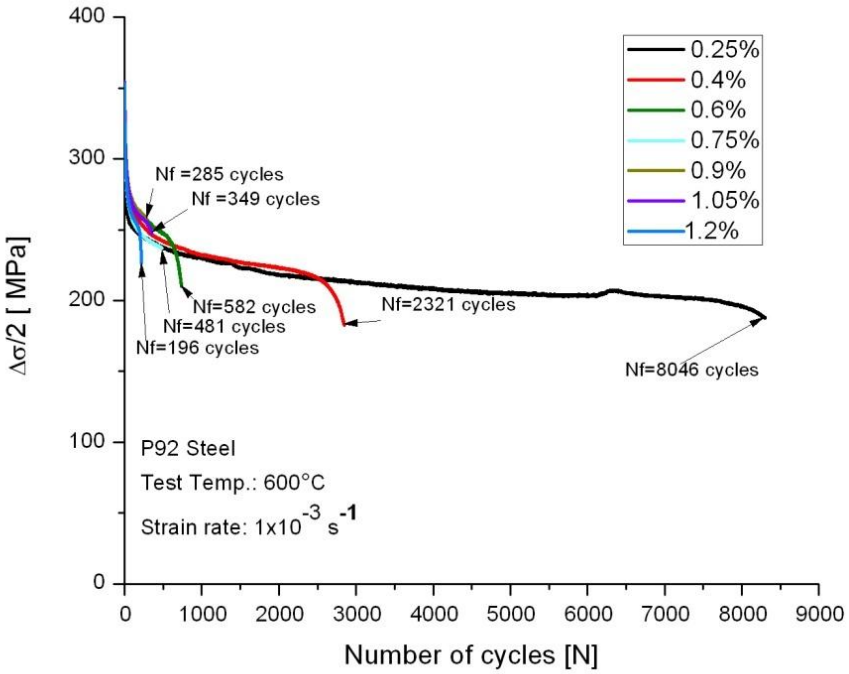

Figure 3.3: Cyclic softening curves obtained from the LCF tests conducted at 600˚C in air on cylindrical specimens for various $\Delta\varepsilon_t/2$ values

Due to the lack of a clear period of stabilization of the hysteresis loop, analytical description of fatigue properties of the examined P92 steel is considerably difficult. Considering the changes observed in the parameters of hysteresis loop ($\Delta\sigma/2$) with the number of stress cycles, the values of hysteresis loop parameters necessary for analytical descriptions of characteristics of the examined P92 steel were determined at $N_f/2^{th}$ cycle.

3.2.2 Hold period test

For the study of time dependent cyclic behaviour, various isothermal creep-fatigue interaction tests were performed by holding at maximum/minimum strain amplitude for 1, 5, 10 minutes. The holding period for the tensile/compressive strain caused a stress relaxation behaviour, which indicates a time-dependency effect for P92 material at high temperature. Creep-fatigue interaction test results and associated parameter are shown in Table3.3.

Figure 3.5, 3.6 and 3.7 show the kind of graph obtained during creep-fatigue interaction for tensile hold, compression hold and combined tension-compression hold respectively. Figure 3.8 shows experimental and modeled stress relaxation curve of 5 minute tensile hold for P92 parent material.

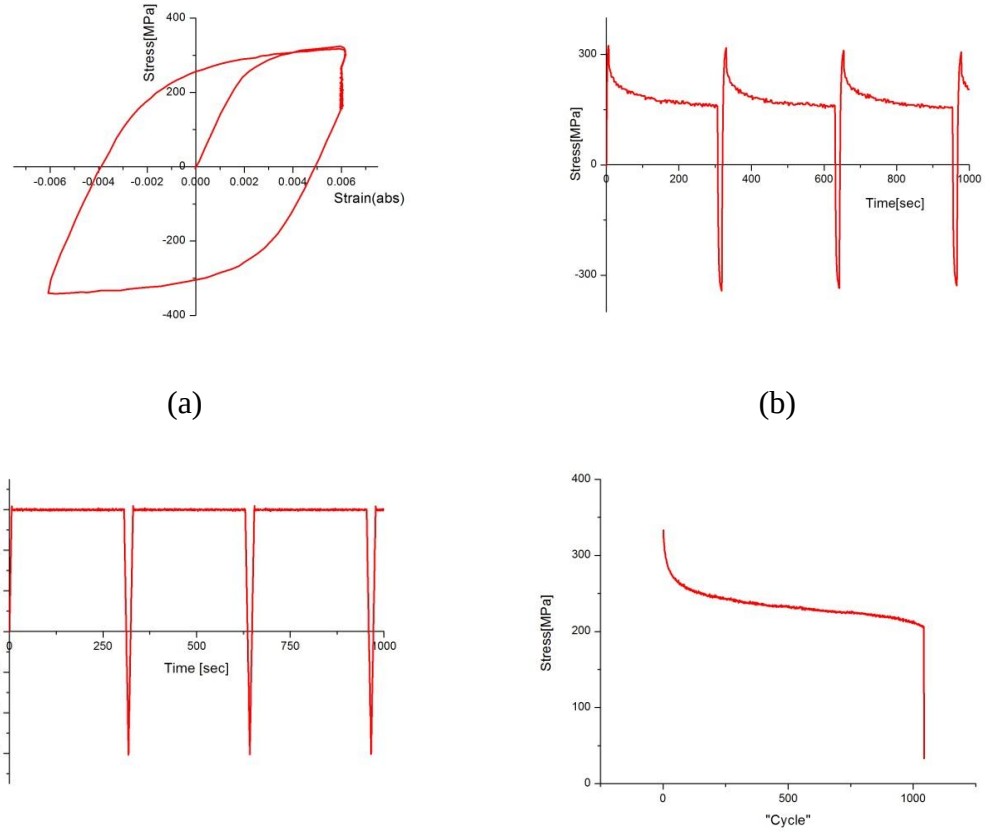

Figure 3.5: Creep-fatigue interaction tests: 5 minute Tensile hold (Strain amp: 0.6%, strain rate:10^{-3} /sec, R = -1, Temp: 600^{0}C).
a) Stress vs Strain graph (Hysteresis loop), b) Stress vs Time graph, c) Strain vs Time graph, d) Stress amplitude vs number of cycles graph

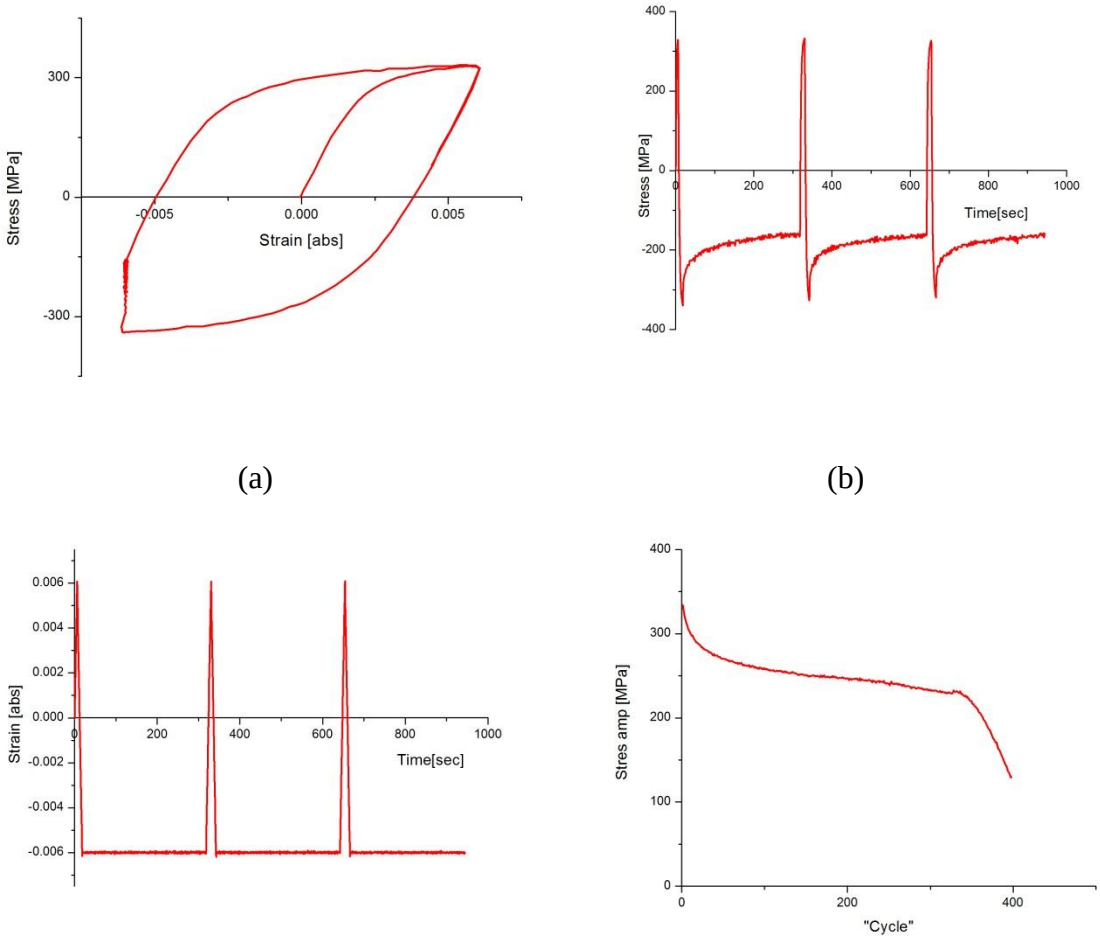

Figure 3.6: Creep-fatigue interaction tests: 5 minute compressive hold (Strain amp: 0.6%, strain rate:10^{-3} /sec, R = -1, Temp: 600^{0}C).
a) Stress vs Strain graph (Hysteresis loop), b) Stress vs Time graph, c) Strain vs Time graph, d) Stress amplitude vs number of cycles graph

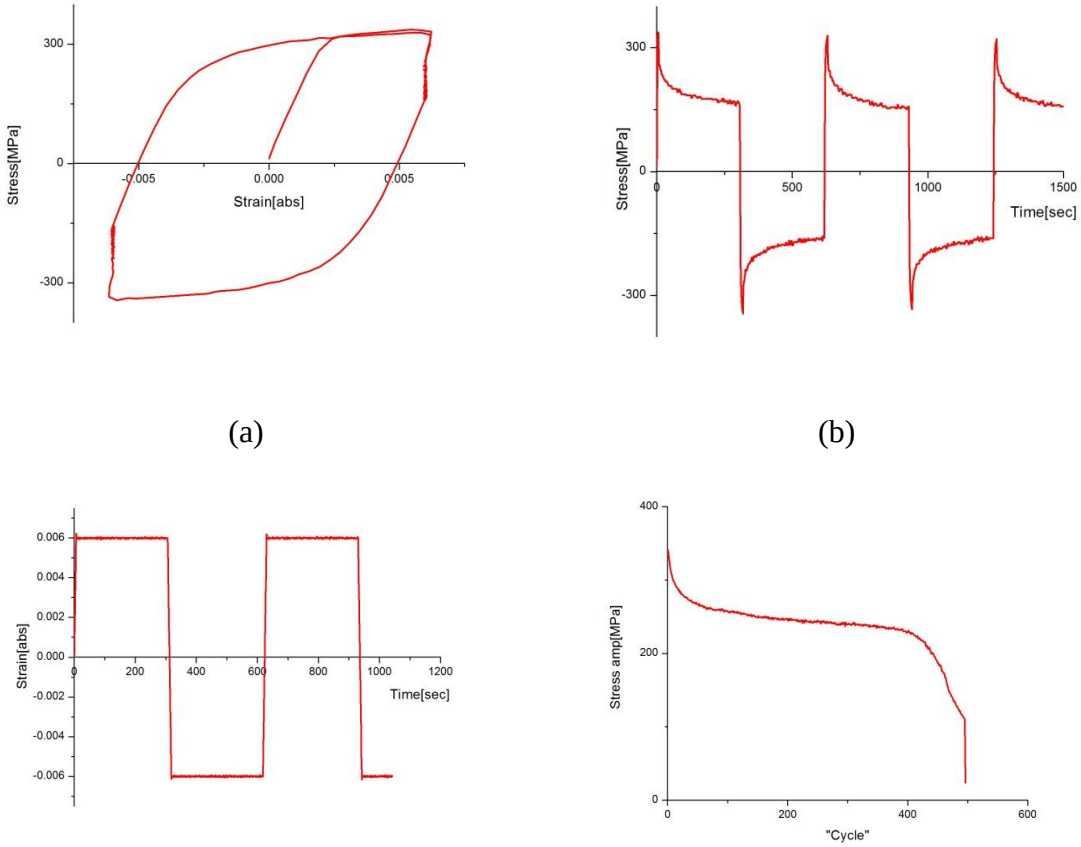

Figure 3.7: Creep-fatigue interaction tests: 5 minute tension and compression hold (Strain amp: 0.6%, strain rate: 10^{-3} /sec, R = -1, Temp: 600°C.
a) Stress vs Strain graph (Hysteresis loop), b) Stress vs Time graph, c) Strain vs Time graph, d) Stress amplitude vs number of cycles graph

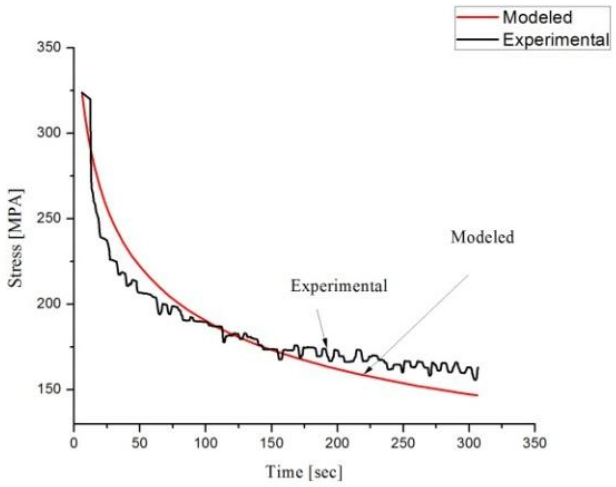

Figure 3.8: Experimental and modeled stress relaxation curve during first cycle of 5 minute tensile hold at strain amplitude 0.6%

Table 3.3

Creep-fatigue interaction tests parameter of various hold time, cyclic life, stress amplitude and plastic strain amplitude values at $N_f/2$ cycles. All tests were conducted at strain rate $1x10^{-3}$/s.

Test type	Test temp [^oC]	Total strain amplitude [%]	Gauge diameter [mm]	Hold time [minute]	No. of cycles to failure [N_f]	Stress amplitude ($\Delta\sigma/2$) at $N_f/2^{th}$ cycle [MPa]	$\Delta\varepsilon_p$ (abs) at $N_f/2$
Tension hold	600	0.6	8.1	1	462	247.31	0.00986
Compression hold	600	0.6	7.95	1	370	244.6	0.0096
Tension and compression hold	600	0.6	7.98	1	496	243.34	0.0101
Tension hold	600	0.6	8.04	5	500	243.29	0.0094
Compression hold	600	0.6	7.98	5	300	250.47	0.0094
Tension and compression hold	600	0.6	8.01	5	336	247.61	0.0104
Tension hold	600	0.6	8.07	10	384	244.71	0.0096
Compression hold	600	0.6	8.05	10			
Tension and compression hold	600	0.6	8.02	10	236	249.49	0.0104

CHAPTER 4 - STRESS - STRAIN ANALYSIS

4.1 Overview

This chapter contains an analysis of the stress-strain behaviour, and its related parameters, produced in strain-controlled tests of P92 steel, at 600°C.

4.2 Stress-strain analysis

Based on the results provided in Chapter 3, the P92 steel exhibited cyclic softening behaviour in all of the tests performed in this study. From the isothermal, strain-controlled tests, at 600˚C, with different strain amplitudes, it can be seen that the material exhibits cyclic softening behaviour as can be seen in Figures 3.3 and 3.4, which present the evolutions of the maximum stress when various plastic strain ranges are applied throughout the tests. The same strain rate of $1x10^{-3}$ s^{-1} was used for all of the tests. Parameters such as Young's modulus, hysteresis loop area and loop shape parameter were determined from the cyclic stress-strain loops; these are analysed in this section.

4.3 Fatigue Model

Based on the number of the cycles to failure obtained in the fully-reversed isothermal strain-controlled tests, with 7 different strain amplitudes, a fatigue life model for the P92 steel, at 600°C, based on strain parameters can be developed. In this study, the fatigue models constants were determined using the number of cycles to failure with a 30 percent stress drop failure criterion.

4.3.1 Strain-based model

Coffin and Manson independently established that the damage parameter in low cycle fatigue failure is plastic strain amplitude ($\Delta\varepsilon_p/2$) and can be linearized on a log–log coordinate with $2N_f$.

The Coffin–Manson relation can be written in the form given in the following equation:

$$\frac{\Delta\varepsilon_p}{2} = \varepsilon_f'(2N_f)^c \qquad 4.1$$

ε_f' is the fatigue ductility coefficient and c is the fatigue ductility exponent. The Coffin–Manson plot is shown in Fig. 8. In the strain amplitude range employed, best-fit lines were obtained and the calculated values of the fatigue ductility coefficient, ε_f' and the fatigue ductility exponent, c are listed in Table 5. Fatigue lifetime of the investigated cast steel is described using the equation

of Manson-Coffin plot. Following observations can be made from the Coffin–Manson (CM) plot:

- The cyclic life is significantly reduced for all values of total strain amplitudes except 0.25% total strain amplitude.

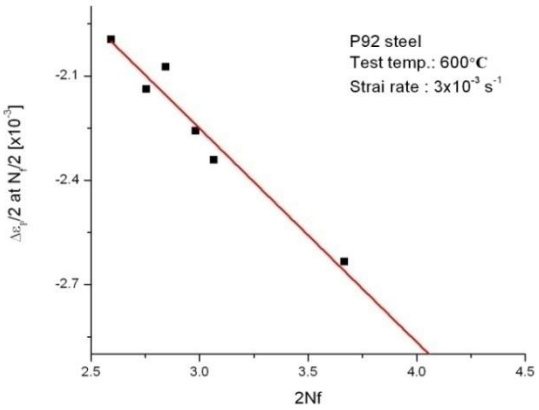

Fig. 8. Coffin–Manson plots obtained from the LCF tests conducted at 600˚C in air at various strain amplitude.

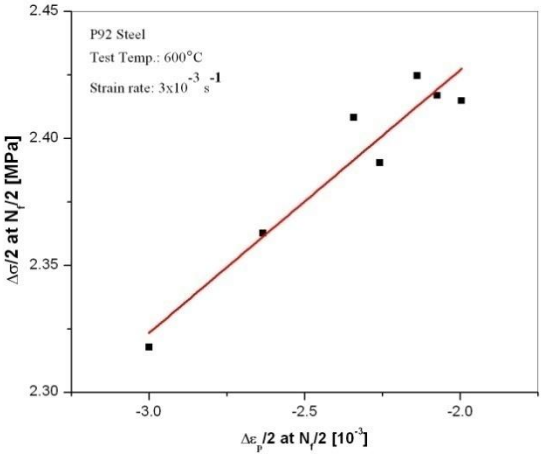

Fig. 9. Cyclic stress–strain curve (CSSC) obtained from the LCF tests conducted at 600˚C in air at various strain amplitude.

Table 5

Calculated values of LCF parameters obtained from Coffin–Manson plot and cyclic stress–strain curve.

LCF parameters	$\varepsilon_f^{'}$	c	$K^{'}$	$n^{'}$
P92 grade steel	0.39	-0.61413	430.7	0.10362

For the analytical description of dependence between stress Δσ/2 and strain Δεp/2, Morrow's equation, as shown below, is applied to obtain cyclic stress strain curve:

$$\frac{\Delta\sigma}{2} = K^{'}\left(\frac{\Delta\varepsilon_p}{2}\right)^{n^{'}}$$

where:

$K^{'}$ is cyclic strain hardening coefficient in MPa;

$n^{'}$ is cyclic strain hardening exponent.

Where, $\Delta\varepsilon_p/2$ is the plastic strain amplitude, $2N_f$ is the number of reversals to failure, ε_f' is the fatigue ductility coefficient and c is the fatigue ductility exponent. Equation 4.6 is based on

Suresh (1998). The ε_f' and c constants can be determined by plotting the log (plastic strain amplitude) against log (number of reversals to failure), as shown in Figure 4.10. The ε_f' and c constants for the Coffin-Manson relationship, determined using parameters at N_{sta}, are 0.5241 and -0.6042, respectively, while the same constants, determined using parameters at $N_{f5/2}$, are 0.4896 and -0.5927, respectively. The figure shows that similar linear relationships are obtained for both types of data; the slope of the N_{sta} graph is slightly higher. The difference between the predicted number of cycles to failure up to 50000 cycles, using both sets of fits to the data, is less than 11 percent.

CHAPTER 5 - VISCOPLASTICITY MODEL DEVELOPMENT

5.1 Overview

The experimental results obtained from LCF and hold time tests are used in this section to develop the material models. A viscoplasticity model has been selected to represent the cyclic plasticity and the time dependent behaviour of the material. The material constants were initially determined by using a step by step procedure. These constants are needed to improve by using an optimization program developed in Matlab in order to obtain better stress-strain predictions.

5.2 The viscoplasticity model

The unified viscoplasticity model, proposed by Chaboche, was chosen here to model the cyclic behaviour of the P92 steel. This model is a time-dependent plasticity model which includes the effects of isotropic and kinematic hardening as well as the rate dependency effects associated with creep. The model is called a unified viscoplasticity model for two reasons: a) there is no partitioning of the inelastic strain into plastic and creep strain components and; b) the hardening rules, which are isotropic and kinematic hardening, are chosen to be similar to the time-independent case [27]. The inelastic strain is also called a viscoplastic strain.

The inelastic strain rate ($\dot{\varepsilon}_p$)of the model is given by the following equations:-

$$\dot{\varepsilon}_p = \left\langle \frac{f}{Z} \right\rangle^n \operatorname{sgn}(\sigma - \chi) \qquad 5.1$$

$$\operatorname{sgn}(x) = \begin{cases} 1, & x > 0 \\ 0, & x = 0 \\ -1, & x < 0 \end{cases} \text{ and } \langle x \rangle = \begin{cases} x, & x > 0 \\ 0, & x \le 0 \end{cases} \qquad 5.2$$

$$f = |\sigma - \chi| - R - k \qquad 5.3$$

where Z and n are material constants; σ is the applied stress; f is the yield function; k is the initial cyclic yield stress, also known as the initial elastic limit, representing the initial size of the yield surface in a deviatoric plane; χ is the kinematic hardening parameter, also known as the back stress; and R is the isotropic hardening parameter, also known as the drag stress [5].

The kinematic hardening model is used to express the behaviour of non-proportional monotonic or cyclic loadings [11]. In a deviatoric stress plane, the kinematic hardening represents a translation of yield surface. Its behaviour is described by the following equation:-

$$\dot{\chi}_i = C_i(a_i\dot{\varepsilon}_p - \chi_i\dot{p}) \qquad 5.4$$

$$\chi = \sum_{i=1}^{M}\chi_i \qquad 5.5$$

Where, i=1,2,…,M ; p is the accumulated inelastic strain; a_i and C_i represent the stationary values of χ_i and the speed to reach the stationary values, respectively. The use of more than one back stress (Equation 5.4) allows a better description of the nonlinear behaviour of a material. In this study, it has been chosen that M = 2 which give the total back stress as follows:-

$$\chi = \chi_1 + \chi_2 \qquad 5.6$$

As the number of cycles increase in a cyclic loading condition, a material may harden or soften with respect to the plastic flow, often as a function of accumulated inelastic strain. This behaviour is represented by an expansion or contraction of the yield surface in the deviatoric stress plane. It is referred to as isotropic hardening due to the fact that it changes uniformly in all directions, in the stress space [24] and is described by the following equation:-

$$\dot{R} = b(Q - R)\dot{p} \qquad 5.7$$

Where, Q is the asymptotic value of the isotropic variable, R, at the stabilized cyclic condition and b governs the stabilization speed.

In the combined isotropic and kinematic hardening of a plasticity model, the applied stress consists of yield stress, drag stress and back stress. Plastic flow occurs when the yield function is equal to zero. For the viscoplasticity model, the plastic yield limit is no longer applied and the load point may lie outside the yield surface. This specific behaviour for the model is represented by a viscous stress (σ_v) as follows:-

$$\sigma_v = Z\dot{p}^{1/n} \qquad 5.8$$

Thus, the applied stress can be decomposed as:-

$$\sigma = \chi + (R + k + \sigma_v)\mathrm{sgn}(\sigma - \chi) = E(\varepsilon - \varepsilon_p) \qquad 5.9$$

The equations described above are in the uniaxial form of the viscoplasticity model which consists of ten temperature dependent material properties, namely E, k, Q, b, a_1, C_1, a_2, C_2, Z and

n. A description of how the constants are determined is given in the next section, using a step by step procedure. Also, the viscoplasticity model, in the uniaxial form, has been implemented in Origin 8 in order to calculate the stress-strain relationship for the steels in tension-compression loading.

5.3 The initial constants of the viscoplasticity model

From the isothermal test data, the test results such as stress-strain data from the first cycle, the evolution of the maximum stress against the number of cycles in a tension-compression test and the stress relaxation data from a dwell test were used in determining these constants. Several assumptions were made during the calculations in order to simplify the equations involved.

5.3.1 Identification of initial yield stress and Young's modulus

Young's modulus (E) was identified from the slope of linear region in the first quarter cycle of the experiment, as shown in Figure 5.1. Generally, the first point to deviate from the linear region is considered to be the yield stress. However, the typical yield stress definition cannot be used in the viscoplasticity model because the yield stress value is higher than an applied stress in a creep test which produces creep strain. As mentioned earlier, the model represents plastic and creep strain in one parameter namely the inelastic strain.

The initial cyclic yield stress, k, value was estimated as suggested by Zhan [49] and as shown in Figure 5.1.

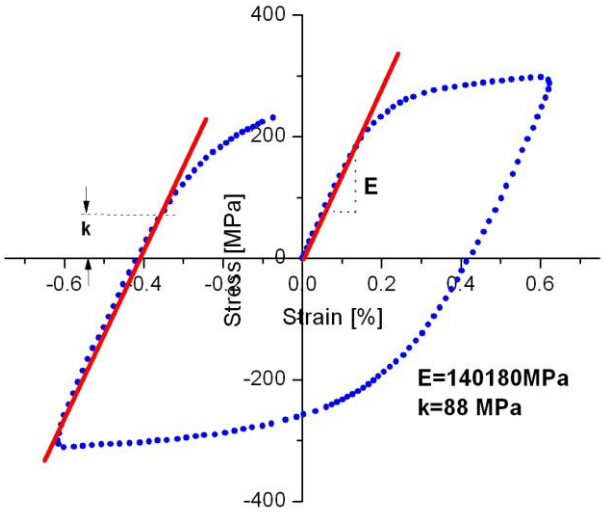

Figure 5.1: Plot for obtaining Young's modulus, E, and estimation of initial cyclic yield stress, k, for the P92 parent material at 600˚C

5.3.2 Identification of isotropic hardening parameters

The evolution of the stress range against number of cycles data obtained from a tension-compression test was used in the determination of the isotropic hardening parameters. All of the test results showed cyclic softening behaviour, in which the stress range decreases as the number of cycles increase, with three different stages. Normally, parameters Q and b are determined by using stress values at a stabilized period in a test where the stress range values become constant. Thus, the stabilized period was assumed to be that at the point at which half of the failure life cycles was produced.

Equation (5.7) can be integrated to give the evolution of isotropic hardening as:-

$$R = Q(1 - e^{-bp}) \qquad 5.10$$

The value of R at a certain number of cycles was taken to be the difference between the maximum stress at that cycle and the maximum stress at the first cycle. Also, the constant Q was taken to be the maximum stress difference between the first and stabilized cycles, which gives a negative value for Q. The parameter p is approximately two times the plastic strain range data for each cycle and its value accumulates as cycles increase. Then, constant b was determined by fitting equation (5.10) to the test data as shown in Figure 5.2.

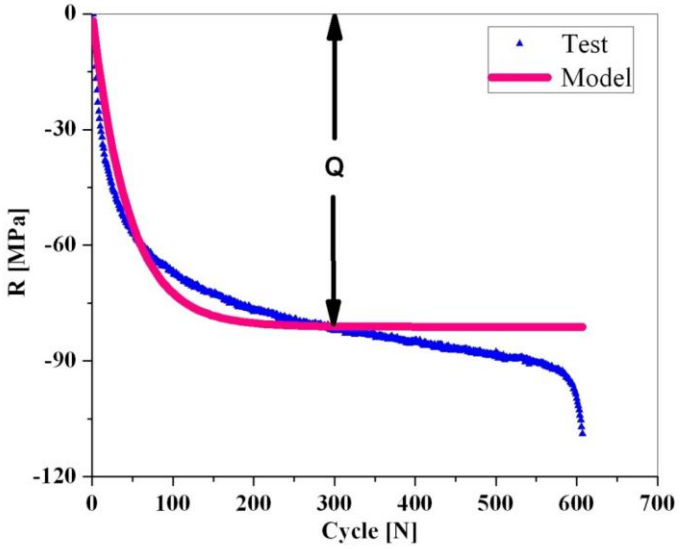

Figure 5.2: Determination of isotropic hardening parameters Q and b for the P92 parent material at 600˚C

5.3.3 Identification of kinematic hardening parameters

Kinematic hardening constants a_1, C_1, a_2 and C_2 were determined using the first-quarter of the first cycle from the tension-compression strain-controlled tests. The non-proportional hardening data of the tensile curve were generally divided into two regions, as shown in Figure 5.3, to represent firstly the transient region of the inelastic deformation, where χ_1 becomes the dominant inelasticity contribution, and secondly the region with greater inelastic strain in which χ_2 is the dominant parameter.

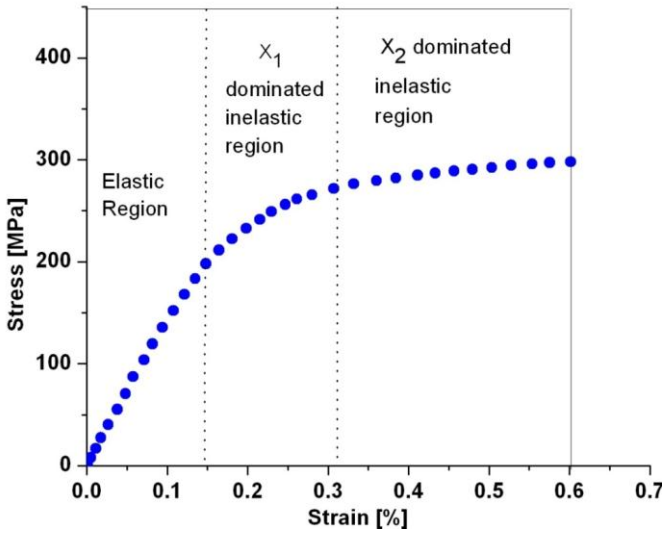

Figure 5.3: Partition of the first quarter of the first cyclic loop for the strain-controlled test data into an elastic region followed by an inelastic region with χ_1 and χ_2 dominated region

Equation (5.4) can be integrated with respect to time to give the following equations:-

$$\chi_1 = a_1(1 - e^{-C_1 p}) \qquad 5.11$$

$$\chi_2 = a_2(1 - e^{-C_2 p}) \qquad 5.12$$

Where, ε_p = p in the first tensile curve data. Equations (5.11) and (5.12) can be substituted into equation (5.9) to give:-

$$\sigma = a_1(1 - e^{-C_1 \varepsilon_p}) + a_2(1 - e^{-C_2 \varepsilon_p}) + R + k + \sigma_v \qquad 5.13$$

Differentiating equation (5.13) with respect to ε_p, by assuming that χ_1 has a negligible effect on the hardening of χ_2 and that k and σ_v are not dependent on ε_p, gives:-

$$\frac{\partial \sigma}{\partial \varepsilon_p} - \frac{\partial R}{\partial \varepsilon_p} = a_2 C_2 e^{-C_2 \varepsilon_p} \qquad 5.14$$

Thus, plotting $\ln[(\partial\sigma/\partial\varepsilon_p) - (\partial R/\partial\varepsilon_p)]$ versus ε_p using data from χ_2 dominated inelastic region, as shown in Figure 5.4, allows the identification of C_2 from the slope of the line and a_2 from the y-axis intercept. In order to plot Figure 5.4 $(\partial\sigma/\partial\varepsilon_p)$ and $(\partial R/\partial\varepsilon_p)$ must be determined first as explained by Hyde [12]. $(\partial R/\partial\varepsilon_p)$ can be calculated based on Equation 5.10. The accumulated inelastic strain (p) parameter in the equation can be substituted ε_p with ($p = \varepsilon_p$ in the first quarter cycle) and the equation can be differentiated with respect to ε_p to give:-

$$\frac{\partial R}{\partial \varepsilon_p} = bQ.e^{-b\varepsilon_p} \qquad 5.15$$

Rearranging $(\partial\sigma/\partial\varepsilon_p)$ by multiplying with (dt/dt) and (dε/dε) gives the following equation:-

$$\frac{d\sigma}{d\varepsilon_p} = \frac{d\sigma}{d\varepsilon} . \frac{1}{\dot{\varepsilon}_p} . \dot{\varepsilon} \qquad 5.16$$

Based on equation (3.16), $d\sigma/d\varepsilon$ and $\dot{\varepsilon_p}$ need to be calculated while the $\dot{\varepsilon}$ value is the controlled parameter in the tension-compression test. In the current model with isothermal application, total strain (ε) is represented by the following equation:-

$$\varepsilon = \varepsilon_e + \varepsilon_p \qquad 5.17$$

In which the elastic strain (ε_e) is equal to σ/E. The inelastic strain rate ($\dot{\varepsilon_p}$) can thus be calculated based on equation (5.17) as following:-

$$\dot{\varepsilon}_p = \dot{\varepsilon}\left(1 - \frac{1}{E}\frac{d\sigma}{d\varepsilon}\right) \qquad 5.18$$

The value of $d\sigma/d\varepsilon$ in equation (5.16) and (5.18) can be calculated using experimental data.

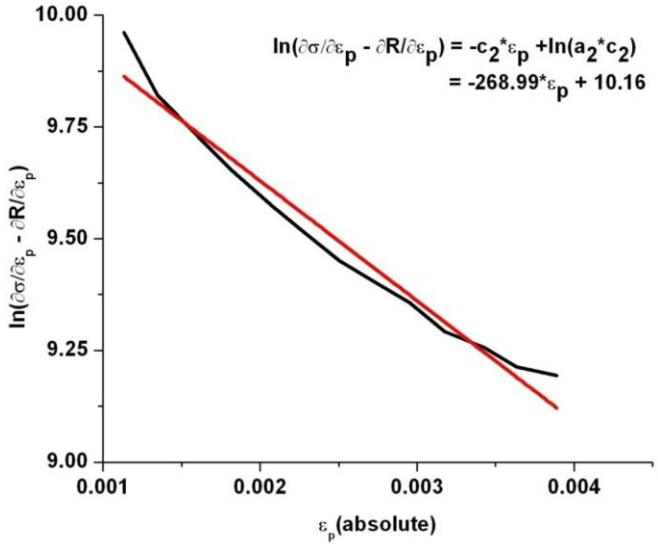

Figure 5.4: Determination of kinematic hardening constants a_2 and C_2 for P92 parent material at 600˚C

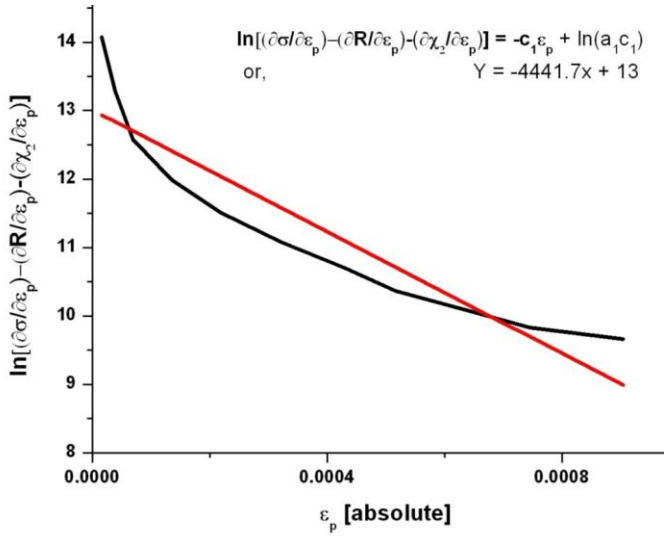

Figure 5.5: Determination of kinematic hardening constants a_2 and C_2 for P92 parent material at 600˚C

On the other hand, as the constants a_2 and C_2 were obtained previously, equation (5.13) can be differentiated with respect to ε_p to give the following equation:-

$$\frac{\partial \sigma}{\partial \varepsilon_p} - \frac{\partial R}{\partial \varepsilon_p} - \frac{\partial \chi_2}{\partial \varepsilon_p} = a_1 C_1 e^{-C_1 \varepsilon_p} \qquad 5.19$$

The constants a_1 and C_1 from the χ_1 dominated inelastic region, can be determined by plotting $\ln[(\partial\sigma/\partial\varepsilon_p)- (\partial R/\partial\varepsilon_p)- (\partial\chi_2/\partial\varepsilon_p)]$ versus ε_p as shown in Figure 5.5. Similar procedures to those described earlier, were used to calculate $(\partial\sigma/\partial\varepsilon_p)$ and $(\partial R/\partial\varepsilon_p)$ for the χ_1 dominated inelastic region data.

5.3.4 Identification of Z and n constants

The viscous constants of Z and n were estimated using the stress relaxation data in the first cycle from the dwell test based on the assumption that the cyclic hardening will not significantly affect the Z and n values. The viscous stress equation can be rearranged to give the following equation:-

$$\log(\sigma_v) = \frac{1}{n}\log(\dot{p}) + \log(Z) \qquad 5.20$$

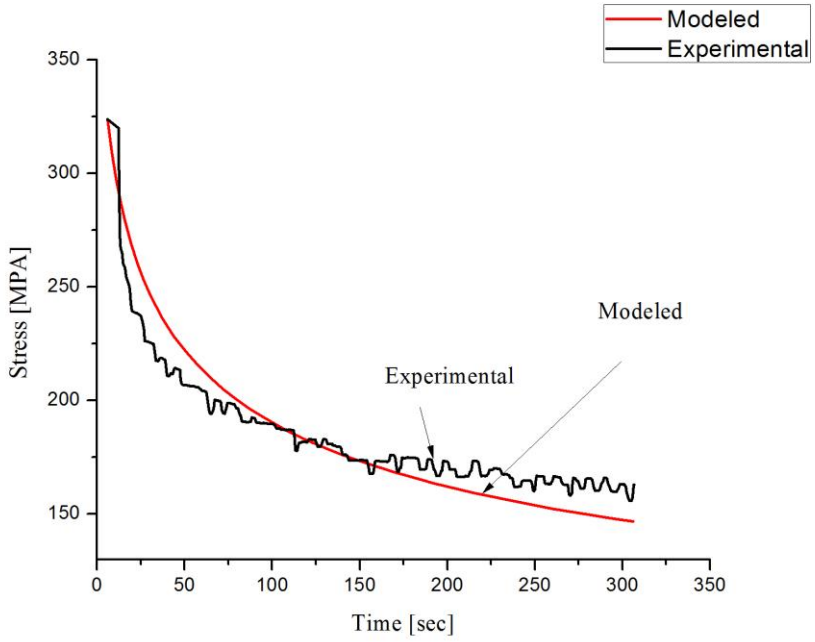

Figure 5.6: Experimental and modeled stress relaxation curve of P92 steel during first cycle of 5 minute tensile hold at strain amplitude 0.6%

In the stress relaxation period, the total strain was held constant and thus the total strain rate equals zero, in which the inelastic strain rate can be determined using the dwell test data by the following equation:-

$$\dot{p} = \dot{\varepsilon}_p = -\frac{\dot{\sigma}}{E} \qquad 5.21$$

On the other hand, viscous stress (σ_v) can be calculated by simplifying equation (5.9), asssuming $\sigma > \chi$ in the first dwell period, and rearranged to give:-

$$\sigma_v = \sigma - \chi - R - k \qquad 5.22$$

By plotting $\log(\sigma_v)$ versus $\log(\dot{p})$ from equation (5.8), as shown in Figure 5.7, the n and Z constants can be identified from the slope of the graph and the y-axis intercept, respectively.

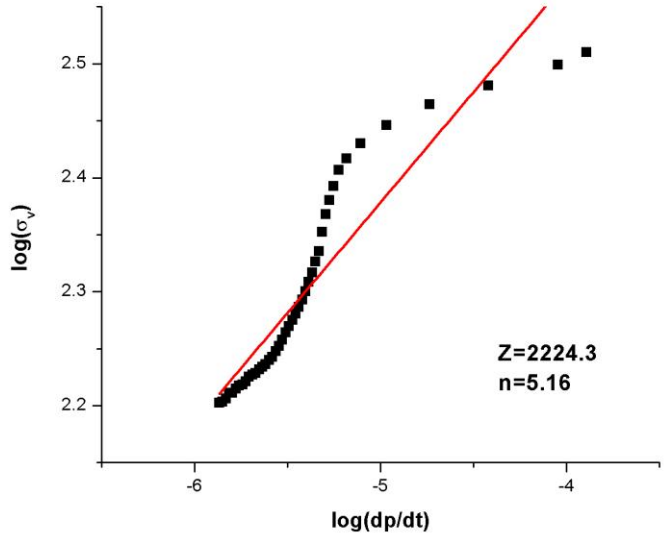

Figure 5.7: Determination of viscous constants Z and n for P92 parent material at 600˚C

The initial viscoplasticity constants for the P92 steel at 600°C temperature, is shown in Table 5.1. These constants are needed to use as the starting parameters in the optimisation process.

Table 5.1 The initial constants of viscoplasticity model for P92 parent material at 600°C

Temp [°C]	E [MPa]	K [MPa]	Q [MPa]	b	a_1 [MPa]	c_1	a_2 [MPa]	c_2	Z [MPa.s$^{1/n}$]	n
600	140180	88	81.16	1.233	95.73	4441.7	93.81	269	2224.3	5.16

Conclusion

- P92 has cyclic softening behaviour as stress amplitude decreases against number of cycle throughout the life of the material.
- There is decrease in the elastic portion of the hysteresis loop which is responsible for cyclic softening and thus the hardening/softening can be explained by change in the size of yield surface in terms of isotropic hardening and kinematic hardening.
- Initial constants can be estimated from tension-compression test data, in which 8 out of 10 constants can be estimated from the first monotonic tensile curve of the first cycle.
- The rest two constants can be estimated from the first stress relaxation curve obtained from the tensile hold data.
-

Future work

Based on the research work presented in this study, some potential work can be further implemented in order to improve and extend the current work in the future are as follows:

- The material initial constants estimated here from the tension-compression test data are needed to optimize further to significantly improve the accuracy of stress-strain prediction of the viscoplasticity model by using non-linear least square method which is an optimization tool in Matlab.
- The finite element simulation, using the viscoplasticity model, need to be implemented in ABAQUS software with an external material library software called Zmat. The simulation results obtained for the steel are needed to compare with the experimental data.

References

1. Ennis, P. J. & Czyrska-Filemonowicz, A. “Recent advances in creep-resistant steels for power plant applications”. Sadhana - Academy Proceedings in Engineering Sciences, 28, 709-730, 2003.

2. Shibli, A. & Starr, F. “Some aspects of plant and research experience in the use of new high strength martensitic steel P91”. International Journal of Pressure Vessels and Piping, 84**,** 114-122, 2007.

3. Hayhurst, R. J., Mustata, R. & Hayhurst, D. R. “Creep constitutive equations for parent, Type IV, R-HAZ, CG-HAZ and weld material in the range 565-640 °C for Cr-Mo-V weldments”. International Journal of Pressure Vessels and Piping, 82**,** 137-144, 2005.

4. Yaguchi, M., Yamamoto, M. & Ogata, T. “A viscoplastic constitutive model for nickel-base superalloy, part 2: modeling under anisothermal conditions”. International Journal of Plasticity, 18**,** 1111-1131, 2002.

5. Chaboche, J. L. & Rousselier, G. “On the Plastic and Viscoplastic Constitutive Equations - Part 1: Rules Developed With Internal Variable Concept”. Journal of Pressure Vessel Technology, 105**,** 153-159, 1983.

6. Sauzay, M., Brillet, H., Monnet, I., Mottot, M., Barcelo, F., Fournier, B. & Pineau, A. “Cyclically induced softening due to low-angle boundary annihilation in a martensitic steel”. Materials Science and Engineering A, 400-401**,** 241-244, 2005.

7. Sauzay, M., Fournier, B., Mottot, M., Pineau, A. & Monnet, I. “Cyclic softening of martensitic steels at high temperature-Experiments and physically based modeling”. Materials Science and Engineering: A, 483-484**,** 410-414, 2008.

8. Lemaitre, J. & Chaboche, J. L. Mechanics of solid materials, Cambridge, Cambridge University Press, 1994.

9. Bhadeshia, H. K. D. H. Mechanisms and Models for Creep Deformation and Rupture. In Milne, I., Ritchie, R. O. & Karihaloo, B. (Eds.) Comprehensive Structural Integrity. Oxford, Pergamon, 2003.

10. Evans, R. W. & Wilshere, B. Creep of metals and alloys, London, Institute of Metals, 1985.

11. Chaboche, J. L. “A review of some plasticity and viscoplasticity constitutive theories”. International Journal of Plasticity, 24**,** 1642-1693, 2008.

12. Hyde, C. J., Sun, W. & Leen, S. B. “Cyclic thermo-mechanical material modelling and testing of 316 stainless steel”. International Journal of Pressure Vessels and Piping, 87**,** 365-372, 2010.

13. Kim, J.-B., Lee, H.-Y., Park, C.-G. & Lee, J.-H. “Creep-fatigue test of a SA 316SS structure and comparative damage evaluations based upon elastic and inelastic approaches”. International Journal of Pressure Vessels and Piping, 85**,** 550-556, 2008.

14. Mannan, S. L. & Valsan, M. “High-temperature low cycle fatigue, creep-fatigue and thermomechanical fatigue of steels and their welds”. International Journal of Mechanical Sciences, 48**,** 160-175, 2006.

15. Leen, S. B., Deshpande, A. & Hyde, T. H. “Experimental and numerical characterization of the cyclic thermomechanical behavior of a high temperature forming tool alloy”. Journal of Manufacturing Science and Engineering, Transactions of the ASME, 132, 2010.

16. Zhan, Z. L. & Tong, J. “A study of cyclic plasticity and viscoplasticity in a new nickel-based superalloy using unified constitutive equations. Part I: Evaluation and determination of material parameters”. Mechanics of Materials, 39**,** 64-72, 2007.

17. Kim, T.-W., Kang, D.-H., Yeom, J.-T. & Park, N.-K. “Continuum damage mechanics-based creep-fatigue-interacted life prediction of nickel-based superalloy at high temperature”. Scripta Materialia, 57**,** 1149-1152, 2007.

18. Yaguchi, M., Yamamoto, M. & Ogata, T. “A viscoplastic constitutive model for nickel-base superalloy, part 2: modeling under anisothermal conditions”. International Journal of Plasticity, 18**,** 1111-1131, 2002.

19. Bernhart, G., Moulinier, G., Brucelle, O. & Delagnes, D. “High temperature low cycle fatigue behaviour of a martensitic forging tool steel”. International Journal of Fatigue, 21**,** 179-186, 1999.

20. Nagesha, A., Valsan, M., Kannan, R., Bhanu Sankara Rao, K. & Mannan, S. L. “Influence of temperature on the low cycle fatigue behaviour of a modified 9Cr-1Mo ferritic steel”. International Journal of Fatigue, 24**,** 1285-1293, 2002.

21. Shankar, V., Valsan, M., Rao, K. B. S., Kannan, R., Mannan, S. L. & Pathak, S. D. "Low cycle fatigue behavior and microstructural evolution of modified 9Cr-1Mo ferritic steel". Materials Science and Engineering: A, 437**,** 413-422, 2006.

22. Fournier, B., Sauzay, M., Caës, C., Noblecourt, M. & Mottot, M. "Analysis of the hysteresis loops of a martensitic steel: Part I: Study of the influence of strain amplitude and temperature under pure fatigue loadings using an enhanced stress partitioning method". Materials Science and Engineering: A, 437**,** 183-196, 2006.

23. Fournier, B., Sauzay, M., Caës, C., Noblecourt, M., Mottot, M., Allais, L., Tournie, I. & Pineau, A. "Creep-Fatigue Interactions in a 9 Pct Cr-1 Pct Mo Martensitic Steel: Part I. Mechanical Test Results". Metallurgical and Materials Transactions A, 40**,** 321-329, 2009a.

24. Dunne, F. & Petrinic, N. Introduction to computational plasticity, Oxford, Oxford University Press, 2005.

25. Zhang, J. & Jiang, Y. "Constitutive modeling of cyclic plasticity deformation of a pure polycrystalline copper". International Journal of Plasticity, 24**,** 1890-1915, 2008.

26. Chun, B. K., Jinn, J. T. & Lee, J. K. "Modeling the Bauschinger effect for sheet metals, part I: theory". International Journal of Plasticity, 18**,** 571-595, 2002.

27. Chaboche, J. L. "Constitutive equations for cyclic plasticity and cyclic viscoplasticity". International Journal of Plasticity, 5**,** 247-302, 1989.

28. Prager, W. "Recent developments in the mathematical theory of plasticity". Journal of Applied Physics, 20**,** 235-241, 1949.

29. Avanzini, A. "Mechanical characterization and finite element modelling of cyclic stress-strain behaviour of ultra high molecular weight polyethylene". Materials & Design, 29**,** 330-343, 2008.

30. Frederick, C. O. & Armstrong, P. J. "A mathematical representation of the multiaxial Bauschinger effect". Materials at High Temperatures, 24**,** 1-26, 2007.

31. Bari, S. & Hassan, T. "Anatomy of coupled constitutive models for ratcheting simulation". International Journal of Plasticity, 16**,** 381-409, 2000.

32. Jiang, Y. & Kurath, P. “Characteristics of the Armstrong-Frederick type plasticity models”. International Journal of Plasticity, 12**,** 387-415, 1996.

33. Chaboche, J. L. “Time-independent constitutive theories for cyclic plasticity”. International Journal of Plasticity, 2**,** 149-188, 1986.

34. Zhao, L. G., Tong, J., Vermeulen, B. & Byrne, J. “On the uniaxial mechanical behaviour of an advanced nickel base superalloy at high temperature”. Mechanics of Materials, 33**,** 593-600, 2001.

35. Shang, J., Leen, S. B. & Hyde, T. H. “Finite-element-based methodology for predicting the thermo-mechanical behaviour of superplastic forming tools”. Proceedings of the Institution of Mechanical Engineers, Part L: Journal of Materials: Design and Applications, 220**,** 113-123, 2006.

36. Krempl, E. “Viscoplastic models for high temperature applications”. International Journal of Solids and Structures, 37**,** 279-291, 2000.

37. Lemaitre, J. Handbook of Materials Behavior Models, Burlington, Academic Press, 2001.

38. Chaboche, J. L. & Gallerneau, F. An overview of the damage approach of durability modelling at elevated temperature. Fatigue and Fracture of Engineering Materials and Structures, 24, 405-418, 2001.

39. Tong, J. & Vermeulen, B. The description of cyclic plasticity and viscoplasticity of waspaloy using unified constitutive equations. International Journal of Fatigue, 25**,** 413-420, 2003.

40. Tong, J., Zhan, Z. L. & Vermeulen, B. Modelling of cyclic plasticity and viscoplasticity of a nickel-based alloy using Chaboche constitutive equations. International Journal of Fatigue, 26**,** 829-837, 2004.

41. Zhan, Z., Fernando, U. S. & TONG, J. Constitutive modelling of viscoplasticity in a nickel-based superalloy at high temperature. International Journal of Fatigue, 30**,** 1314-1323, 2008.

42. Richardot, D., Vaillant, J. C., Arbab, A. & Bendick, W. The T92/P92 book, Vallourec & Mannesmann Tubes, 2000.

43. Ennis, P. J. & Czyrska-Filemonowicz, A. Recent advances in creep-resistant steels for power plant applications. Sadhana - Academy Proceedings in Engineering Sciences, 28, 709-730, 2003.

44. Bendick, W., Cipolla, L., Gabrel, J. & Hald, J. New ECCC assessment of creep rupture strength for steel grade X10CrMoVNb9-1 (Grade 91). International Journal of Pressure Vessels and Piping, 87**,** 304-309, 2010.

45. Swindeman, R. W., Santella, M. L., Maziasz, P. J., Roberts, B. W. & Coleman, K. Issues in replacing Cr-Mo steels and stainless steels with 9Cr-1Mo-V steel. International Journal of Pressure Vessels and Piping, 81, 507-512, 2004.

46. Brett, S. J. UK experience with modified 9Cr (grade 91) steel. VTT Symposium (Valtion Teknillinen Tutkimuskeskus), 1**,** 48-60, 2007.

47. Vaillant, J. C., Vandenberghe, B., Hahn, B., Heuser, H. & Jochum, C. T/P23, 24, 911 and 92: New grades for advanced coal-fired power plants--Properties and experience. International Journal of Pressure Vessels and Piping, 85**,** 38-46, 2008.

48. Igarashi, M. Alloy design philosophy of creep-resistant steel. In Abe, F., Kern, T.-U. & Viswanathan, R. (Eds.) Creep-resistant steels. Cambridge, Woodhead Publishing, CRC Press, 2008.

49. Zhan, Z. A study of creep-fatigue interaction in a new nickel-based superalloy. University of Portsmouth, 2004.